UNIVERSIDADE
BEIRA INTERIOR

Mechanical Performance Optimization of Bonded Composite Patch Repairs: a flexural analysis

Francisca Sá Ferreira

Dissertação para obtenção do Grau de Mestre em
Engenharia Aeronáutica
(mestrado integrado)

(Versão final após defesa)

Orientador: Prof. Dr. Paulo Nobre Balbis dos Reis
Co-orientadores: Prof. Dra. Sofia Teixeira de Freitas e Dr. Mohamed Nasr Saleh

Fevereiro de 2021

Acknowledgment

The conclusion of this work was only possible thanks to the collaboration and support of several people and institutions. I would like to thank the University of Beira Interior and the Delft University of Technology and the people that work in these institutions for providing the facilities, materials and equipment necessary to fulfill the objectives of this work.

However, there are people whose contributions were indispensable to the completion of this work and to whom I owe a lot: I would like to thank to my thesis supervisor, Professor Paulo Nobre Balbis dos Reis, for his support, teachings and all the personal time that he dedicated to this work. I would also like to thank Professor Sofia Teixeira de Freitas for the opportunity of expand and develop my knowledge and tools in a new and developed environment that allowed me to learn not only about my own work but also about many other approaches of numerical and experimental studies. To Mohamed Nasr Saleh, I would like to thank for the support, availability, teachings and major contribution in all aspects of this work, for always being willing to help and allow me to produce the best work I was capable of.

Finally, I would like to thank my mother, family, boyfriend and friends for the patience and support during harder times, and I am glad I could share this experience with you.

This Master Dissertation has been supported by the project Centro-01-0145-FEDER-000017-EMaDeS- Energy, Materials and Sustainable Development, co-financed by the Portugal 2020 Program (PT 2020), within the Regional Operational Program of the Center (CENTRO 2020) and the European Union through the European Regional Development Fund (ERDF).

Cofinanciado por:

Resumo

Os efeitos da sequência de empilhamento ($[0,90,0,90,0,90]_S$ ou $[90,0,90,0,90,0]_S$) e das dimensões do remendo (30, 40 ou 60 mm) foi estudada, tal como a sensibilidade do laminado de controlo ao furo de 20 mm de diâmetro. De forma a compreender estes efeitos, testes quase estáticos de flexão em três pontos foram desenvolvidos para avaliar a rigidez à flexão e capacidade de carga das amostras reparadas. Os espécimes foram impactados a baixa velocidade com o objetivo de estudar a influência das variáveis estudadas relativamente ao dano e propriedades residuais. Foram dinamicamente testados em testes de fadiga com flexão em três pontos para verificar a tendência dos efeitos de fadiga dependendo das dimensões do remendo. A análise numérica de elementos finitos foi validada. Verificou-se que os laminados de controlo, para ambas as sequências, são sensíveis ao furo de acordo com as condições estudadas. Para as amostras com orientação 0º (identificação relativa à orientação da camada mais externa dos laminados), o remendo de 60 mm revelou-se como uma reparação eficaz, já que as propriedades mecânicas originais foram restituídas. Nenhum dos remendos estudados foram considerados como sendo reparações válidas para as amostras de 90º. O dano obtido por impacto, com uma energia de 12J, foi inversamente proporcional ao aumento do tamanho do remendo, para as duas sequências, visto que o remendo de 60 mm apresentou dano em menos de 25% da sua área total. A degradação por fadiga, por ação de cargas de fadiga, mostrou-se proporcional às dimensões do remendo, sendo que o remendo de 30 mm apresentou o maior número de ciclos de vida, para ambas as orientações. Os mecanismos de dano gerais foram consistentes para os testes quase estáticos e dinâmicos, sendo que os nos espécimes 0º a rutura final foi a delaminação interlaminar no remendo e, para os laminados 90º, a delaminação verificou-se na lamina externa do laminado de controlo, devido à ação do remendo e adesivo a arrancar fibras dessa mesma lamina na direção transversal. Por último, foi provado que o adesivo não representa o elemento mais fraco em nenhuma das reparações, sendo que a falha ocorreu sempre em um dos laminados.

Palavras-chave

Reparação em Remendo; Fibras de Carbono; Compósitos; Sensibilidade ao Furo; Fadiga; Laminado de Controlo; Sequência de Empilhamento; Flexão; Impacto

Abstract

The effect of the stacking sequence ($[0,90,0,90,0,90]_S$ or $[90,0,90,0,90,0]_S$) and patch size (30, 40 or 60 mm) were studied, as well as the notch sensitivity of the parent plate to a 20 mm diameter hole. For this purpose, quasi-static three-point bending tests were performed to evaluate the bending stiffness and load-carrying capacity of the repaired structure. The FE numerical analysis was validated. The specimens were also low-velocity impacted in order to evaluate the influence of the studied variables in the damage mechanisms and residual properties. The specimens tested in three-point bending fatigue to verify the tendency of the fatigue effects depending on the patch dimensions. It was observed that the parent laminate, for both stacking sequences, is notch sensitive according to the studied conditions. For the specimens with 0º outermost ply, the 60 mm patch was revealed as an effective repair as its mechanical properties were restored. However, none of the studied patch sizes were considered as a valid repair for the 90º specimens. The impact damaged relative area, caused by an energy level of 12J, was inversely proportional to the increase of patch size,for both orientations, as the 60 mm patch presented a damage under 25% of the overall patch area, while the 30 and 40 mm presented damage in 38 to 50% of the overall patch area. The fatigue degradation, when exposed to fatigue loading, was found to be proportional to the patch size, as the 30 mm patches for both laminate types presented longer life cycles, 3933 for the 0º specimens and 6599 for the 90º cycles, while for the other patch sizes the maximum of life cycles were around 1667. The overall damage mechanisms were found to be consistent for the quasi-static and dynamic tests, as for the 0º specimens the ultimate failure was found to be the interlaminar delamination in the patch and, for the 90º specimens, the delamination was verified in the outermost ply of the parent laminate, due to the patch and adhesive pulling the ply yarns oriented at the transverse direction. Finally, the adhesive was proven not to be the weakest link in any of the repairs, as the failure damage was always verified in one of the composite laminates.

Keywords

Bonded Patch Repair; Carbon Fiber; Composites; Notch Sensitivity; Quasi-Static Tests; Dynamic Tests; Fatigue; Parent Laminate; Stacking Sequence

Contents

List of Figures

List of Tables

Acronyms

BVD	barely-visible damage
BVID	barely visible impact damage
CFRP	carbon fiber reinforced polymer
CLT	classical lamination theory
FE	Finite element
FEA	finite element analysis
FEM	finite element method
FOD	foreign object damage
PAN	polyacrylonitrile
SLJ	single-lap joint
UBI	Universidade da Beira Interior
VSTOL	vertical short take off and landing

Nomenclature

d	patch length
D	diameter
E	Young's modulus
g	gravity acceleration
H	height
L	span
N	number of load cycles
P	force
P_{max}	maximum load
S	fatigue stress
t	thickness
t_{max}	maximum thickness
W	width
δ	displacement
ε	elongation
σ	stress
σ_n	notched strength
σ_{un}	unnotched strength

Chapter 1

Introduction

Composite materials are in constant evolution, as new applications are constantly being explored, however their economic and technological importance is already established. Several industries highly depend on the use of composites in order to satisfy their needs, specially to achieve high stiffness and strength values but with a limitation of weight. These industries are as diverse as aerospace and defense, equipment and appliances, construction, electric and electronic, marine, transportation, pipes and tanks, medical and prosthetic and renewable energies, among many others [**?**, **?**, **?**, **?**]. However, these industries also suffer a large pressure relative to the air pollution, global warming and other environmental subjects that have a big importance in the present times. Therefore the weight reduction is associated as a solution in response to these problems, with the possibility of improving and replacing certain materials in order to cope with the increased need of recycling end-of-life vehicles and with other waste management regulations imposed by the governments.

When talking about the evolution of composite materials in the aerospace industry, the boosting period was unmistakably during the Cold War, period from which the development and research about new composites consolidated [**?**]. Nowadays, commercial aircraft as the Boeing 787 and A350 were able to save in weight by substituting primary structures made of aluminum alloys with composite parts [**?**]. During operational life and maintenance activities the structures and equipment are always exposed to damage. Delamination, fiber breakage, matrix cracks or debonding, between the laminates and the adhesive, are typical damage mechanisms that highly affect the resistance and stiffness of composite structures. These damages may be cause by impact or fatigue, as studied in this work, which compromise the integrity of the composite and possibly leave a barely visible damage [**?**, **?**, **?**, **?**].

Depending on the severity of these damages, the need of repair or replacement can arise. Most parts made of composite materials used in aircraft are costly which is why most replacements are nonviable and only used as a last option. For smaller and localized damages, the isolation and repair of the damaged area allows a faster and cheaper method, without compromising the integrity of the part. The bonded repairs are widely used in this industry, and when the damage is of difficult access, the single patch repairs become the most efficient way of restoring the mechanical properties of the structure. These repairs become responsible for supporting the stresses, the temperature variations and the chemical environments that they are exposed to during service. These repairs allow an on-site

temporary repair in order to prolong the structure's life up to the moment of ultimate repair or replacement, and their efficiency depends on several aspects as geometry, dimension, adhesive material used, laminates' stacking sequence and others [**?**, **?**, **?**, **?**, **?**, **?**].

Alongside with this method, the removal of the damaged area by drilling an open hole around it, to avoid propagation in the parent laminate, is a common procedure, which also influences the design and quality of the repair. An open hole on the parent laminate results in high stress concentrations around its edges and the need of predicting the effects on the laminate strength, highly dependent on the hole geometry [**?**, **?**].

Finally, and as these repairs are expected to bare the same conditions as the original structures, it is important to subject them to similar tests, low-velocity impact and fatigue, and investigate their behavior and response in order to ensure an efficient repair [**?**, **?**, **?**, **?**, **?**, **?**, **?**, **?**].

In this work, and according to the multiple variables that influence the optimization of single patch repairs, a flexural study was conducted in order to evaluate the effect of the stacking sequence of both the parent and patch laminates and the effect of the dimension of the square patch in restoring the resistance and load-carrying capacity of the structure. In the first four chapters, the theoretical concepts, industry overview and state of the art, necessary for the understanding of this work, are presented. In the fifth and sixth chapter, the experimental and numerical approaches, materials, equipment and procedures will be explained. Finally, the results of the study are presented and discussed, followed by the final conclusions and suggestions for future work.

Chapter 2

Composites

A simplistic definition of composite materials is as a combination of two or more materials that together form an odd combination of properties. One of the first examples of this concept is the wood, that combines cellulose fibers with lignin, a natural glue, however there are much more examples of composites found in the nature, as shells from molluscs that were found to be much stronger than some man-made composites [**?**].

From a very early stage, it was found that combining different materials could be advantageous when trying to achieve greater properties to those of the individual components. These combinations are vast from bricks reinforced with straw, in Egypt, to the construction of bows with the bonding of wood pieces and cattle tendons that was steamed and bent into the desired shape, wrapped with silk thread and later slowly cooled, in Mongolia. A wide variety of materials can be classified as composite materials, such as fiber reinforced plastics, regular and steel reinforced concrete, particle filled plastics, rubber reinforced plastics, wood laminates and ceramic mixtures. As this concept is far from narrow, it is commonly assumed, and specially in this work, that terms as ”composites” and ”composite materials” are being used with a restricted connotation as only fiber reinforced materials, being defined as solid materials composed of a binder or matrix that surrounds and holds in place reinforcements [**?**].

The main material which properties compete with structural composites are metallic materials, however, and looking to satisfy industries as aerospace, the former presents lower densities, high specific strength, high specific modulus and great fatigue damage tolerance [**?**]. When comparing these two categories of materials, each one represents a wide group of several materials, however the comparison does not fail as the data correctly reflects the general trends [**?**].

Fiber-reinforced composite materials can be defined as fibers that are bonded or incorporated in a matrix, presenting different interfaces between them, but maintaining their physical and chemical properties that, conjugated, become an unique combination of characteristics that can not be found in any of them individually [**?**]. The supporting structures can be fibers, particulates or whiskers and made from polymers, ceramics and metals, while the matrix can be from metals, plastics or ceramics. The most common composite materials used nowadays are the ones made with matrix based on polymer-resins, which is the category where this work will lay on, essentially [**?**].

Usually fiber-reinforced composites are used in the form of laminates, that consist in the stacking of a number of layers of the fibers and resin, with the goal of achieving a specified thickness. In this process, one of the main parameters to define is the orientation of the fibers in each ply in order to create the most beneficial structural properties for the composite laminate according to its duty. This is extremely relevant as mechanical and thermal properties, as tensile strength and modulus, have a high dependency on the direction of the fibers, therefore usually a multidirectional stacking that despite having lower properties than the longitudinal stacking, represent the best option as in real life applications it is expected a state of multi-axial loads, resembling the isotropy of metals [**?**].

2.1 Matrix

The matrix provides rigidity and environmental resistance, which maintains the placement of the fibers, transfers stresses between the fibers, protects the structure from chemicals and moisture and prevents the mechanical degradation [**?**].

As a compound resultant of the combination of a resin and a filler, which behaves as a homogeneous material, it is responsible for the ability of the composite material to operate in a specific operating temperature and also the manufacturing process [**?**, **?**].

The matrix can be classified as polymeric, metallic or ceramic. As the ones used in this specific work, polymer matrices can also be called as resins or plastics, and as the name indicates, refers to the junction of many individual molecules that form a chain-like structure where each unit is like a link in the chain. Polymers are found in mixtures of many similar chains all intertwined. They usually have long chains and even when presenting only a few units, they have the tendency to join with others in order to form longer ones [**?**].

The resins can be categorized as thermoplastic, after molded or manufactured they can be reprocessed as many times as needed which allows it to have a lower cost, or thermosetting, with only one possibility of processing, presenting better thermomechanical properties and being the most used in composite materials [**?**].

In the thermoplastic materials,commonly called as plastics, the molecules are joined by weak secondary bonds or intermolecular bonds that temporarily separate in the presence of heat, move to a new configuration with the pressure and solidify in the cooling process, allowing the reprocessing of the material [**?**]. The interest in this type of materials is based on their low cost from the availability of the materials and of the manufacturing processes but also teamed with its low mechanical and thermomechanical properties. Applied in the composites manufacturing, its use is limited because of the use of high temperatures

to produce the final products [**?**]. Another major issue is the higher viscosity of the thermoplastic resins compared to thermosetting, making it difficult to use them as matrix of high-performance composites because it complicates the impregnation process.

The thermosetting materials present a high number of cross-links which provides the resin a higher rigidity and thermal stability.During the curing phase, these high levels of cross-links are being formed which counterworks the possible melting of the material by the application of heat. However, the thermoset polymer can possibly be soften ,under elevated temperatures, if the number of created cross-links is lower than normal [**?**]. These resins have three possible classifications, polyester resins, condensation resins or epoxide resins, the type of resin chosen for this work and the most used in the aeronautical and space industry for its high performance [**?**].

As a versatile system, presenting low shrinkage and excellent adhesion, epoxies are the most widely used thermosetting resins in a big variety of applications. They are extremely versatile, from being able to adapt the formulation or combine different materials, properties can be changed and improved, according to the epoxy's application [**?**].

An epoxy is composed by multiple epoxide groups, which are three-member rings of one oxygen atom and two carbon atoms, defining the start material that can be mixed with other materials in order to reduce viscosity, by diluents, or improve the impact strength of the cured matrix, by flexibilizers [**?**]. The epoxies are then cured by chemical chemical reaction with curing agents, just before the addition of fibers in the liquid mix, and then the cross-links start to form, three-dimensional, until the resin solidifies. All this being adaptable in order to satisfy the required properties.

Epoxies provide good performance at room and high temperatures, up to 76.85 ºC to 116.85 ºC, or more specific epoxies can go up to 203.85 ºC which cost is higher but, as high performance epoxies, they provide good corrosive and chemical resistance [**?**].

Epoxy matrix overtakes other thermoset matrices for its wide variety of properties, the non-existence of volatile matters during cure, low shrinkage, high resistance to chemicals and excellent compatibility with fillers, fibers and substrates [**?**].

Reinforced epoxy resins in laminate sheets, that represent 25% of the total of all epoxies produced, stand out in the market of electrical circuit boards for their inherent low conductivity and high dielectric strength combined with their low tendency to emit gases even when subjected to an electrical discharge. They also have a relatively good thermal stability of epoxies, excellent adhesive properties and good mechanical properties which led to their high utilization in high performance composites, mainly in the ones that use carbon or graphite as their reinforcement [**?**].

2.2 Fibers

Reinforcements can be classified as fibers, whiskers or particles, which the former one represents oblong fibers compared to the other dimensions that are often circular or near circular. This relation between length and width or height is expressed mathematically as the aspect ratio, that is the ratio of the length to the diameter of a fiber. Fibers have high aspect ratios, which allows the transfer of loads along the long axis and gives them the efficiency needed in a composite structure [**?**].

As the main portion of volume of the composite material and responsible for most of the rigidity [**?**], parameters as the fibers' type, length and orientation have an huge influence in the following characteristics of the composite laminate, density, tensile strength and modulus, fatigue strength and fatigue failure mechanisms, electrical and thermal conductivity and cost, therefore, depending on the application of the material, the fibers' parameters must be properly selected. Table 2.1 compares several properties of different fiber types [**?**].

Table 2.1: Typical properties of some polymeric fibers [**?**].

Material	**Density** (g/cm^3)	**Tensile Modulus** (GPa)	**Tensile Strength** (GPa)	**Specific Modulus**	**Specific Strength**	**Melting Point** (ºC)	**Elongation at break** (%)
E-glass	2.54	70	3.45	27	1.35	1540+	4.8
S-glass	2.50	86	4.50	34.5	1.8	1540+	5.7
Graphite, high modulus	1.9	400	1.8	200	0.9	>3500	1.5
Graphite, high strength	1.7	240	2.6	140	1.5	>3500	0.8
Boron	2.6	400	3.5	155	1.3	2300	-
Kevlar 29	1.45	80	2.8	55.5	1.9	500(D)	3.5
Kevlar 49	1.45	130	2.8	89.5	1.9	500(D)	2.5

The fibers are the main carrier of the load, provide stiffness, strength and other structural properties and insulating or conducting energy, depending on the fiber [**?**]. A fiber has a diameter of a few microns and is considered a elementary filament, used in groups as strands or yarns [**?**].

As the type of fibers chosen to this work, carbon fibers are advantageous for their high tensile strength-weight and tensile modulus-weight ratios, their dimensional stability because of a low coefficient of linear thermal expansion, high fatigue strength, and high thermal conductivity. They have its niche of applications where the weight and performance are critical parameters, which justifies the high cost of the material, usually in the aerospace industry [**?**].

The carbon atoms are arranged in hexagonal structures organized by crystallographic planes, between each planes the carbon atoms have weak bonds which provides the good thermal and electrical conduction properties while in the same plane the bonds are strong

that allow the graphite its high mechanical properties [**?**].

This fibers can be manufactured from textile or pitch precursors,through thermal processes, being the most common of the latter one the polyacrylonitrile (PAN) [**?**]. The precursors go through three main operations, oxidation by high temperatures with the goal of supressing the melting point, carbonization, improving the cross-links with high temperatures, graphitization, increasing the Young's modulus but with reverse effects on the ultimate strength. A fourth procedure can also be used, the surface of carbon fibers are exposed to an acid atmosphere in order to achieve a higher level of adhesion between the fibers and matrix. While PAN-based fibers are the most used in the fabrication of carbon fibers, pitch fibers, that are originated from the refining of petrol or oil, tend to have significant advantages as high weight efficiency, a ratio of fibers/precursor of 75% to 80% compared to the 50% ratio of the PAN process, a faster graphitization and a cheaper raw material [**?**].

The mechanical properties of carbon fibers are considered very good, specially as they are maintained up to around 1500º, which has allowed the development of composites with high temperature behavior in nonoxidizing atmosphere, used in rocket nozzles, break blocks and others, but also easily combined with antioxidant layers for applications in more oxidant environments as space [**?**].

2.3 Prepregs

As resin-impregnated fibers, orientated at 0º, created for later use in a hand lay-up or mold, where the resin is partially cured or thickened. The prepregs are unidirectional, which allows the capacity of adapting the directions and in turn, adapting also the composite properties. Each type of prepreg, assigned for the type of resin used, differs in features as drape, the ability to take a different shape of the mold, or the tackiness, the stickiness when uncured. Specifically, the thermoset prepregs have an easy drape and enough tack, however have some restrictions as a defined shelf life and the need to be stored in lower temperatures to avoid the resin curing (6 to 8 days at 23 ºC or 6 months at -18 ºC) [**?**, **?**].

Preimpregnated forms of high performance fibers with a thermosetting resin, usually epoxy, are used in structural applications, after being cured with application of specific values of heat and pressure [**?**]. Usually, the prepreg contains higher quantities of resin than needed, which removal helps with the extraction of air bubbles that could affect the final product, and allows the reduction of weight. This avoids possible gaps that reduce significantly the interlaminar shear strength, for 1% of voids there is a reduction of 7%, and the compressive strength, for lacuna's percentages higher than 2%. More recent prepregs are already made with the quantity of resin near the quantity desired in the final laminate

by using hot melt impregnation [**?**].

Prepregs surpass metals for higher specific stiffness, specific strength, corrosion resistance and easier manufacturing, regardless of its higher cost for the higher fiber volume fraction [**?**].

2.4 Manufacturing Process

Selecting the manufacturing process depends on three different factors, type of matrix and fibers, necessary temperature to cure the matrix and form the laminate and the cost effectiveness of the process. During the design of any composite structure, the choice of the material and manufacturing is made simultaneously as the designer needs to understand the particular limitations of both. Therefore, there are multiple processes as hand layup, prepreg layup, bag molding, autoclave processing, compression molding, resin transfer molding, vacuum-assisted resin transfer molding, pultrusin and filament winding, among others. Specifically used in this work, and therefore those which will be talked more in-depth, are the prepreg lay-up and autoclave processing [**?**].

A process of composite manufacturing involves specific operations, independently of different processes, varying only the way used for each operation and, in some cases, some steps are preformed simultaneously. These operations are placing the fiber according to the desired orientations, impregnating the fibers with resin, consolidation the impregnated fibers and remove the excess resin, cure and solidification of the polymer, extracting the mold and finally finishing operations [**?**].

The prepreg layup includes cutting the prepreg according to the required geometry and dimensions, laying the different plies down following the desired orientations on a tool, apply a vacuum bag technique and finally putting all inside an autoclave where heat and pressure are applied for the curing process. The parameters for this process depend and must be in agreement with the manufacturer recommendations, from a full or partial vacuum within the bag, a wide array of pressure values (higher than the atmospheric pressure) to be applied to the interior of the pressure vessel and the temperature that is raised to achieve the cure of the polymer. The curing cycle and consolidation of the laminate in an autoclave is long and extensive [**?**].

2.4.1 Laminates

A laminate consists of the overlapping of plies of the fibers saturated with resin, for example, layers of prepregs. These laminates result of the stacking of many unidirectional

plies considering different orientation of the fibers according to the desired mechanical properties and are identified by a code associated to each orientation and the thickness, specifying the orientation of each layer according to a fixed system of axes, their symmetry if existent and different layer's materials in case of hybrid laminates [**?**].

The main factors to be considered in the choice of the type of laminate and sequence to be created ,specifically applied to this work, are the good mechanical properties measured in the direction of the fibers in an unidirectional layer and the sensitivity of a cross-ply laminate to interlaminar delamination [**?**].

Chapter 3

Composites History and Market

When it comes to the history of the considered modern composites, it is estimated that the starting point was around 1930 when, almost accidentally, an engineer became intrigued with a fiber that was being formed during the process of lettering in a glass bottle. The initial product obtained from this fine drawn molten glass was insulation, however structural products soon followed. A couple of years later, a salesman from the Owens-Corning Fiberglass Company started to sell fiberglass to different costumers around the United States and those started to realized that it could be used as reinforcements. The aircraft industry stood out as a potential costumer for the new material, as small aircraft companies were in constant creation of new designs and concepts in manufacturing of aircraft, this represented also the possible need of new materials. Douglas Aircraft was the first company to buy a roll of fiberglass as it was expected to be the solution to their production problems. The design innovations implied the need of new metal molds which were expensive and had a slow production, leading to the desire of using plastic molds, however these were not able to endure the forces of metal-forming process. Therefore, they started successfully using plastic molds reinforced with fiberglass to make a few parts in order to verify and approve them, and later produce the metal dies for the full productions runs. Around the same period, also unsaturated polyester resins and higher performance resins became available, establishing an even development between materials and applications [**?**].

By World War II, composites development increased even more, beyond being used in tooling they started to be used in structural and semi-structural parts of airplanes. Can be considered as an example the ducts that were one of the last parts of an aircraft to be designed, which implied the need of being designed in accordance to other existing parts twisting and turning around them, positioning ducts in difficult to access locations. For this shapes, composites became the perfect solution. With the high demand of materials, the US became concerned with the availability of metals for aircraft, increasing the effort to create design rules and manufacturing methods for composites as a substitute to metals. Several design concepts and manufacturing methods were validated including the development of filament winding and spray-up, sandwich structures, fire-resistant composites, and prepreg materials [**?**].

After the end of the war, it came to the point that many companies had developed expertise and they had to target potential markets and products, some of the developments were able to be converted directly from war applications to commercial applications, as

fiberglass reinforced polyester boats. Other than the direct reapplications, the automobile was the most logical applications of composites, leading to the creation of a completely composite automobile body. Some products made during this era still represent the major markets for composite materials nowadays [**?**].

For the last seventy years, the volume and number of applications for composite materials have emerged and conquered a wide variety of markets. The reason for this noticeable growth is based on the achievement of unique mechanical, physical and thermal characteristics, as a final product that is lighter and stronger. Being now a material that is applied in most industries, by the year 2000, the transportation industry stood up as the largest user for the material, with a consumption of 1.3 billion pounds (approximately 590 million kilograms) of composites [**?**,**?**,**?**]. In Figure 3.1 the current demand of carbon fibers and the expected growth are shown.

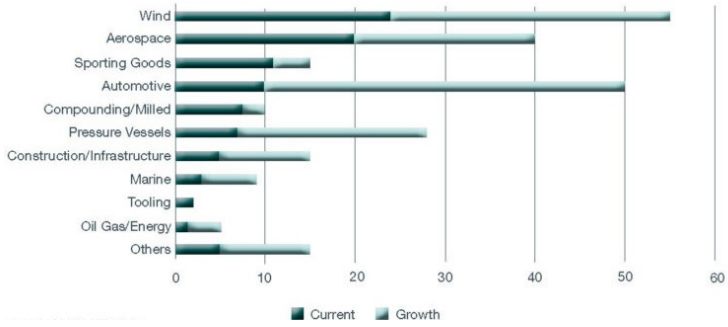

Figure 3.1: Current demand of carbon fibers for several industries and expected growth [**?**].

In order to meet the diversified market needs, advanced manufacturing technologies and material systems were developed, therefore several industries have capitalized on the benefits of composites. The main factor that contributed to this clear expansion was the decrease of the fibers' cost allied to the development of automation techniques and high volume production methods [**?**].

The Composites market can mainly be divided into the following industries: aerospace, automotive, construction, marine,corrosion resistant equipment,consumer products, appliance/business equipment, medical and prosthetic industries, oil and gas sector, renewable energy industry and others [**?**].

The aerospace industry, as described before, was one of the firsts to become aware of the potential of composite materials and the possible achievement of faster, higher and further flights from its airplanes, rockets and missiles and with the introduction of carbon fibers in the 1970s, carbon fiber-reinforced epoxy has become the primary material in many wing, fuselage,and empennage components. By 1999, the aerospace industry was consuming 23 million pounds of composites (approximately 454 thousand kilograms) [**?**].

Considering military aircraft, as F-11,F-14,F-15 and F-16, the use of composites focus on the purpose of reducing the weight of the structure, and are present in structure as

horizontal and vertical stabilizers, wing skins, fin boxes, flaps, and various other structural components, expressing reductions on the range of 20 to 30% on the mass of the components and allowing the optimization of the missile range and/or increase of the payload. There are also examples of aircraft which airframes contain 25% by weight of carbon fiber-reinforce polymers, as the AV-8B, a vertical and short take-off and landing (VSTOL) aircraft introduced in 1982 and the F-22 fighter aircraft. Furthermore, the outer skin of B-2 and other stealth aircraft is almost totally made of composites, which grants them the stealth characteristics when combined with special coatings and other features that help to reduce reflection and heat radiation [**?**].

When it comes to commercial aircraft, Airbus was the first manufacturer to make extensive use of composites in their A310 aircraft, introduced in 1987, already representing 10% of the total aircraft's weight. From this and over the years, the utilization of composite materials in different parts of the aircraft only increased, mainly up to 2006 with the Airbus A380 which had 25% of its weight made of composite, highlighting the main parts as the central torsion box, rear-pressure bulkhead, tail and the flight control surfaces.In the meantime, Boeing started to make use of composites in the empennage, control surfaces, engine coolings and fuselage floor beams, which can be observed in the Boeing 777, since 1995, that has a 10% of its structural weight made of carbon fiber-reinforced epoxy and other 50% made of aluminum alloys, being that the percentage weight of composite parts also increased in the aircraft models later developed and presented, always aiming to lower the weight in order to increase the payload and the fuel efficiency [**?**].

On the other hand, in spacecraft applications, the material choice is due to weight savings but also dimensional stability. In low Earth orbit, with temperature variations between -100 to 11 ^{o}C, it is important to ensure dimensional stability in support structures and reflecting members. For example, carbon-epoxy composite laminates can be designed in order to give a zero coefficient of thermal expansion. The most common composite structures in spacecraft are tubular truss structures, facesheets for the payload baydoor, antena reflectors and others, and this applications represent , in space shuttles, savings of 2688 pounds (approximately 1.2 thousand kilograms) per vehicle [**?**].

Other than weight saving and its consequent optimization, there are some other advantages in using fiber-reinforced polymers over aluminum and titanium alloys, that are transverse to most industries. From the possibility of reduction in the number of components and fasteners that helps reducing fabrication and assembly costs, to the higher values of fatigue resistance and corrosion resistance that decrease the maintenance and repair costs and, finally, the capacity of aeroelastically tailoring the stiffness of an airframe structure during the laminate construction process. In Figure 3.2 examples of composite structures used in commercial aircraft are shown [**?**].

In general, the primary restriction to the use of composites is their high initial cost compared to other materials. This happens because regardless of the effectiveness of the

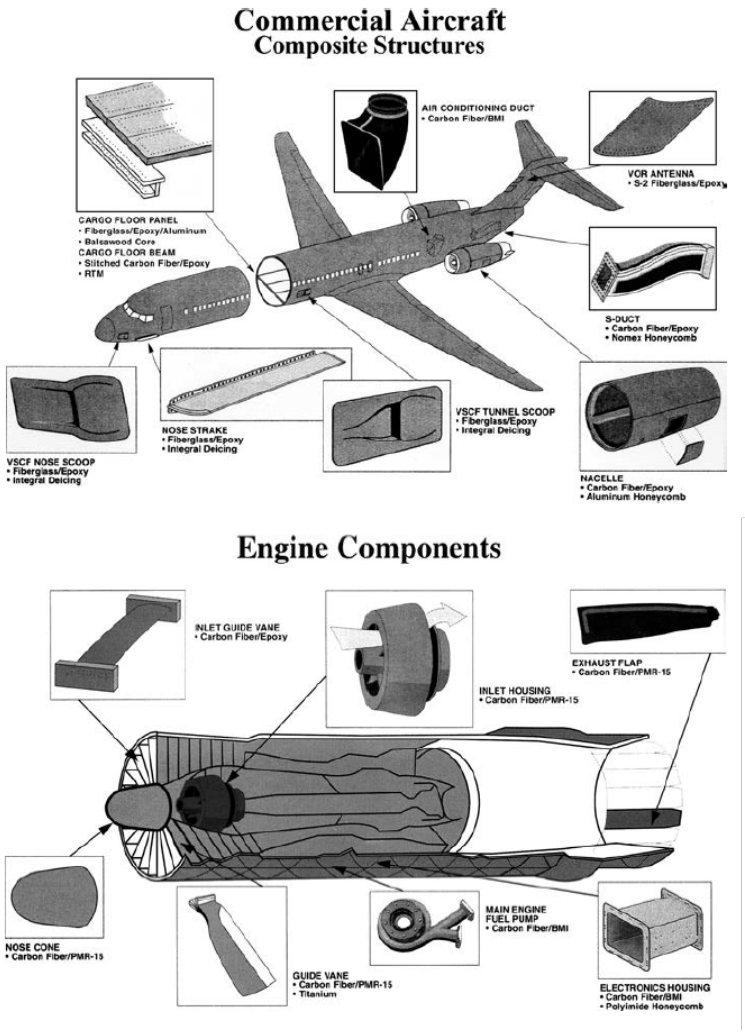

Figure 3.2: Examples of composite structures used in aircraft [**?**].

material over its lifetime, the industry considers high upfront costs specially when the life cycle cost is relatively uncertain, limiting the research into new materials. The cost of processing composites is high, in this manufacturing process the raw material costs represent only a small fraction of the total cost, specially in the hand lay-up process. Recycling of a composite material is also a possibility, however this becomes a problem and limitation when it comes to a high-volume market, where volume production is millions of parts per year [**?**].

Nowadays, the aerospace industry remains one of the primary users of composite materials, being expected that the increasing use of carbon fibers in aircraft combined with the rising number of aircraft launched in the market each year will represent a huge growth opportunity for the carbon fiber market specifically, between 2019 and 2024. According to the Boeing's Commercial Market Outlook 219-2038 report, the air travel market is projected to be 2.5 times bigger in the next two decades, which represents the need to produce and deliver more than 44000 jets. These predictions, as an aggressive demand in aerospace, lead to a clear need, for the composites industry, to not only improve their

material development and supply but also improvement of manufacturing processes and engineers equipped with advanced hybrid, scalable, flexible and extensible tools to adapt to growing complexities [**?**].

Chapter 4

State of the Art

The wide use of fiber reinforced composites creates the need to develop repair techniques for structures made of such composites [**?**]. These structures of external use are susceptible to foreign-object damage (FOD), from bird strikes to tool drops, which can induce interlaminar delamination, matrix cracking and fiber breakage, damage modes verified during this study, reducing the residual strength and stiffness of composite laminates. Some damages can be produced by in-service events, as careless handling, or interaction and contact with attached or connected structures as pillars and bends. These damages can often go undetectable by visual inspection of the laminate, being considered as barely-visible [**?**].

To improve the structural integrity of a damaged component and ensure service life safety, the damaged should be repaired or entire damage structure should be replaced. The choice between these two options depends on several considerations, such as the location of the damage in the structure itself, thickness, aerodynamic requirements, operation conditions, weight, mechanical property requirements and damaged area or extent of the damage. Most of the aircraft structures fabricated using composite materials represent high costs, which leads to the adoption of repair techniques to recover the damaged components without compromising the original mechanical integrity. In cases where the replacement of complex integrated structures is unnecessary due to a minor damage, repair becomes a cost reduction way of enhancing service life of components [**?**].

For general damages in aircraft, a structural repair manual, given by the manufacturer and approved by a regulatory authority, has most of the data needed to perform a repair operation, in case of a damage size contained by the restrictions. Otherwise, with a larger damage size, the repair becomes dependent of an engineering assessment by the relevant authority. The sequence of restoration of the structures is to identify the damage, quantify the damage by nondestructive inspection, dress the damage, perform the repair operation and finally restore aircraft surface finish.These techniques have been developed in order to repair specific parts and structures with specific materials for the aerospace field, usually not being applicable to the general material or different applications. In order to achieve the goal of creating standard repair procedures for composite structures, it is important to understand the different factors that influence the effectiveness of the repair and obtain repeatable data that indicates how these factors can affect the strength of the repaired part [**?**, **?**].

Each part of a structure is designed to have a specific strength when the $1g$ loads are multiplied by factors considered necessary for safety. They must be strong enough to resist the maximum tensile, compressive and bending loads likely to be applied to them in the worst design case. As an example of this, the fuselage must not twist excessively when a maximum rudder deflection is applied, as the wing when applied an aileron. The ability of a repair to carry the same or greater load as the original is an important consideration. This laminate strength is often evaluated according to the ultimate stress capability of the laminate, which represents the maximum loads considering a safety factor [**?**].

When a repair operation takes place, it is important to recognize the nature and amount of damage of the component. The damage is evaluated using several inspection techniques in order to determine the necessary means to restore and achieve the strength, reliability, performance, safety and durability as near as the ones of the undamaged structure. Some of the main considerations taken into account for the overall process of repair are the time of operation, the smoothness in the case of outer surfaces (fuel saving) and the weight balance in control structures but also in the general components, being restricted to defined limits and possibly needing rebalancing of the structures [**?**].

The strength and stiffness of a composite repair depend on the type of raw materials, geometric factors and processing factors that are employed in the repair.The design parameter of composite repairs must guarantee that the repaired region uniformly transfers the service loads under service conditions. The design is also responsible to ensure that the residual strength of the repaired structure is higher than the unnotched strength of the parent laminate, which allows failure to initially happen in the laminate instead of the repair. The amount of material to be removed from the parent laminate for a patch repair operation relies not only on the extend of the damage but also on the geometric factors of the patch [**?**].

For some parts, it is important to meet stiffness requirements in order to also meet the strength requirements. A structure may be strong enough to bare the loads applied to it, however it is needed to control the deflection under the load so it meets its function and mechanical operation. If the stiffness is inadequate, flutter may occur, for example, if a resonant frequency is reached due to a turbulent airflow, and the part may fracture quickly due to fatigue. The inverse may also happen if the torsional stiffness of a wing is not sufficient to meet the loads applied by an aileron deflection at high speeds [**?**].

The comparative stiffness between an original and a repaired laminate is an important repair design consideration and may be as near to the original as possible. This stiffness is related to the Young's modulus (E) and is the slope of the linearly elastic section of a material's stress-strain curve. This slope is the ratio between the applied stress (σ) and the resulting strain (ε) (Equation 4.1). This relation is plotted for a given material such that the strain, under stress conditions, is known throughout the linear elastic region. Composite laminate stress-strain curves are typically a straight line limited as a linear elastic

behavior. A material whose stress-strain linear elastic slope is steeper has a higher modulus of elasticity and therefore will have a higher stiffness. Because of this, the Young's modulus of the parent and repair materials must be adjusted, according to the thickness, to achieve a comparable section stiffness, $(E * t)$ [**?**].

$$E = \frac{\sigma}{\varepsilon} \quad (4.1)$$

The damage nature of composite materials mainly relies on environmental service conditions and strain rates. Failure in composite laminates can be at laminate level (interlaminar delamination), lamina level (fiber pullout, fiber-matrix debonding, matrix-cracking or fiber breakage), or structure level (failure in the component). Mainly, when talking about impact loads,the failure is induced in the subsurface of the laminate, at the interlamina and intralamina levels, with only minimal surface failure. Damage can also be induced from environmental factors such as rain erosion, hail, ultraviolet radiation, lightning strikes and moisture ingression. Due to all these factors, aircraft-maintenance checks are moderate when it is in service condition, performed without dismantling and according to two different levels A and B, or detailed when the aircraft is temporarily out of service, C level checks with dismantling. The maintenance relies on the flight hours and flight cycles. The maintenance, repair and overhaul market is responsible for the significance of aircraft reliability and safety [**?**].

Interlaminar delaminations form at the interface between the plies of the laminate and they may initiate from matrix cracks that progress to the interlaminar ply. The severity of this type of damage is dependent on the width and length dimensions of the laminate, the number of delaminations in that specific area, the location of the damage and especially on the loads under which the structure is subjected. The latter is relevant because delamination behavior relies on the type of loading, having little influence when loaded in tension but , when under shear or compression loading, possibly progressing to an unwanted load redistribution mechanism that can lead to reduced stiffness or strength and possible structure failure [**?**].

On the other hand, fiber breakage becomes critical as composites are often fabricated as fiber dominant, however this type of damage is limited to the impact area and constrained by the impact energy and object [**?**].

When the damage is considered minor, which is a common event, a simple cosmetic repair may be used, as filling the damaged area with epoxy (no need to remove the affected sites). These minor damages do not immediately affect the structural integrity of the structure, however they can result in an abrupt progression of the damage. Otherwise, bonded and bolted repairs are adopted in cases of critical damage, as they allow an uniform load transfer over and around the repaired region. In critically damaged structures, the damaged area must be removed before the repair operation is performed [**?**].

One of the most well-accepted repair performed on all types of fiber-reinforced polymers is external patch repair, as a very simple and cost-effective procedure that requires the least amount of preparation. This repair can be permanent or temporary, depending on the type of patch that is used, but also is practical for urgent in situ repairs. In adhesively bonded patch repair technique, the damaged area in the parent laminate is removed, usually by drilling a hole, possibly filled with resin, and then a fiber-reinforced polymer patch is applied. The choice of turning the damaged/cracked into a circular hole is related to the goal of avoiding possible singular stresses in the cracked region. The patch repair technique is frequently adopted to repair damaged laminates for its low consumption of time and low cost but also for the circumstances when the accessibility to both sides of the structure is not possible [**?**, **?**].

Adhesively bonded patch repairs are suitable for thin plates, allowing their bonding with least stress concentrations and minimal disturbances in the aerodynamically flush area. It is also advantageous as these repairs can represent a low weight enhancement and a certain control of the stiffness, however the materials used for processing and fabrication are highly responsive to environmental conditions, as temperature and humidity. The main limitations of this process is the size-constrain, as for deep damage repair, a high amount of material is needed and the temperature of the repair region needs to be evened, but also for the need of frequent inspections. Following these considerations, patch repairs are suitable for secondary components but not for a primary aircraft component as it is difficult to assure the bond quality in order to evaluate durability and strength without the use of destructive testing [**?**].

The joint between the two adherents in the adhesively bonded repair is created using an adhesive material. In this work, an epoxy adhesive is used, considering that thermosetting epoxies are the most common among the adhesives. Epoxy adhesives can be one or two components and can be cured both in ambient and high temperatures, however, in order to produce better mechanical properties at elevated temperatures, the ambient ones must be post cured. A two-component epoxy blend comprises a curing agent, a resin and possibly additives. In order to have a good adhesion it is important to improve molecular contact and provide close contact between the adhesive and the adherents. Surface roughening prior to the bonding is also important to enhance the strength of the bond. The capacity of the bonds to withstand stress and the quantity of plastic deformation define the energy of adhesion. With a good adhesion, the joint fails only cohesively, in cases that the properties of the joint rely on the properties of the adhesive, if the adherent materials are stronger than the adhesive [**?**].

During the process of bonding the different parts, it is possible to obtain different standard configurations to be employed to the industry. It is possible to create a spew, when squeezing the adhesive at the joint, creating a fillet of adhesive that surrounds the full thickness of the patch. The adhesive can also be applied in both surfaces, patch and parent laminate, obtaining maximum shear strength [**?**].

In order to investigate adhesively bonded repairs, numerical and analytic methods are used. Nowadays, the majority of analytic models used for bonded repairs are two-dimensional (2D), neglecting the stress produced in the third direction. Furthermore, most of investigations are linear elastic for both adhesive and adherents as geometric behavior and non linear materials are difficult to include in analytic models. Computational approach offers a tool to perform analysis of arbitrary loading conditions and geometries, being employed in order predict critical stress sites by nonlinear analysis. Modeling approaches based on fracture and damage mechanics can be used to analyze the effect of various design factors on the failure behavior and joint strength. However, intricate material models are necessary in order to analyze the structural damage behavior of composite repairs subject to various service conditions. In these analyses, the difference of dimension between the patch and the bondline must be taken into consideration. Finite element (FE) models provide the opportunity to investigate the difference in the joint strength and to find critical process factors. Using these numerical models, it is possible to design and optimize bonded patch repairs, but it is important to know the details of mechanical properties of each repair material [**?**, **?**].

When it comes to the dimension of the repair area this must be studied according to the data of the component to be repaired, accessible area of the joint, and the needed area to achieve the load transfer. Several bonded patch repair configurations are configured depending on the bond strength and most favorable overlap length obtained from lap-shear tests, however this method leads to the false notion that the shear stresses generated in the repair are even. In the joint, high shear stresses are situated at the edges of the overlap length, while low shear stresses at the middle. Davis and Bond studied several basic principles for overall adhesive repairs. They revealed that increasing the overlap length just reduces the stress concentration however it has no influence on the residual strength. The bonded joints may also be designed so the adhesive sustains higher loads compared to the original structure, so the adhesive never fails [**?**].

Single lap joints are commonly used to measure the bond quality of a repair, however this type of bonded repair has two disadvantages, the addition of stress components by the offset of substrates and the peak stresses at the edges , resulting in an uneven distribution of stress in the overlap. This has been studied over the last sixty years to estimate the distribution of stress in the repair and aiming an optimization of a favorable bonded patch repair configuration [**?**].

During the design phase of the adhesive joint, the joint geometry must be studied in order to avoid undesirable stresses that could cause premature failure in the adhesive or adherends. Hart-Smith [**?**] proposed a guideline for the selection of joint configurations according to the size of the composite adherends. The single-lap joints (SLJ) are considered the weakest configuration due to the eccentric load path. Other joint configurations, as double-lap or scarfed joints, represent a higher and more balanced strength when used in thin adherends. However, the higher strength values also represent higher costs and

manufacturing difficulty, which must be taken into account when low levels of strength is adequate. After determining the overall configuration, the strength can be further improved by smaller modifications as local modification of adherends and/or adhesive. This is usually performed at the edges of the overlap, where there is a higher stress concentration. The single-lap joint is based on one adherend overlapped and bonded to a parent structure. Increasing the overlap length of this repair does not represent an increase in the failure load, possibly hitting a maximum when a certain overlap length is reached. There are common shear and peal stress concentrations, and this can be revealed by an optimization of the shape of adherends, specially at the edges [**?**].

Within SLJ repairs, adherend shaping is a good way to decrease the stress concentration at the edges of the overlap in order to uniformly distribute the load transfer, reducing the local stiffness of the joint in these areas. Tapering of the adherend decreases the stiffness of the laminate edges and hence the discontinuity at the extremities of the bonded area. Haghani et al. [**?**] performed a numerical study that indicated that the effect of tapering on the stress distribution is highly dependent on the stiffness of the laminates and the adhesive used. This is more effective when performed in softer laminates. Inside tampering was found to be more favorable than outside. These optimization techniques are also commonly used in composite repair patches at the overlap lengths or with the creation of fillets with the adhesive itself, preventing failure induced by peel stresses at the edges [**?**, **?**, **?**].

Chue et al. [**?**] used 3D finite element model, linear elastic fracture mechanisms and strain energy density theory to study the effects of size and stacking sequence of a rectangular patch. Increasing the patch size reduces the strain energy level at the crack tip. This increase is more favorable when applied to the length of the patch than to the width (dimension parallel to the considered crack). Considering a 3-ply patch, arranging the sequence has little influence on the strain energy distribution near the crack tip. Furthermore, in bonded repair damage in aircraft components under variable loads, the ideal orientations of the patch, relatively to the crack direction, are 90 and 45. High effective stresses in the adhesive are observable in the edges of the patch and may cause the patch to debond.

Early works of Soutis and Hu [**?**] examined the compressive behaviors of patched CFRP laminates and concluded that the performance of a repair depends strongly on the structural coherence between patch, parent laminate and adhesive. In their study, and considering circular patches, they defined that with a safety factor in view of possible effects as poor bonding, patch delamination and enirnmental effects, a thin plate with a 20 mm hopen hole, the patch should have a diameter of 60 to 80 mm. On the other hand, the thickness of the patch, and therefore its stiffness, must be taken into consideration so the peel stresses don't become limiting to the joint strength and causing failure without experiencing high through-thickness tensile strength. Liu and Wang [**?**] investigated composite laminates with circular patches under static tensile loading using finite element

analysis (FEA). Their work studied the effect of patch size on the ultimate strength and failure mechanism. For repairs with 40 mm diameter, with an small overlap length, there is high stress concentration in that small area, which leads to fast propagation and finally to detachment of patch and laminate, sue to shear failure in the adhesive. Specifically in this work, and for a hole with 30 mm, patches larger than 50 mm show no shear failure occurring in the adhesive, and for bigger patches the failure progress is more stable and slow. Finally, when talking about the effects of stacking sequence, it showed little influence on the failure strength and also in the failure mechanism. Except for the fact that matrix cracking is more likely to initiate in 90º laminates, near the hole edges. Reis and Antunes [**?**] considered a similar situation, but using single-lap tensile loaded joints where, using a 2D finite element model was used and analyzed the influence of the overlap length on the joint failure. According to them, the overlap length of 30 mm showed the lower values of equivalent stress, correspondent to failures loads obtained experimentally. Furthermore, the variation of superposition length represented considerable change in the equivalent stresses value, being considered as a damage criterion for those types of single-lap joints.

Caminero et al. [**?**, **?**] studied single- and double-patch repairs in composite panels under tensile loading. Nondestructive testing techniques were used to monitor and study damage, as Digital Image Correlation, Ultrasonic guided waves, X-ray radiographs and ultrasonic C-scanning. Gong et al. [**?**] developed a generalized optimization model of bonded circular patch repairs according to the location of damage initiation and its process of evolution, that depend on the patch configuration. This optimization is dependent on the balance of the stress distribution at the longitudinal edges of the patch and transversal edges of the hole. Her and Chao [**?**] studied the stress analysis of an adhesively bonded repair using FEA. The damage was simulated as a circular hole and the efficiency of a square patch repair was evaluated by a comparison of the stress concentration factor before and after the repair. The numerical analyses defined conclusions as the thicker and stiffer the patch, the more load is transmitted to it, which leads to a better efficiency, the increase of the adhesive thickness results in a decrease of stress concentration factor, however the shear modulus of the adhesive leads to the opposite, and finally the patch has more influence on the repair than the adhesive.

Akpinar [**?**] subjected six different types of double-strap joint, five of them with composite patches with different orientations, to a bending test. Laminate patches with each stacking sequence, $[90]_{16}$,$[0]_{16}$,$[0/90]_{8}$,$[45/\text{-}45]_{8}$ and $[0/45/\text{-}45/90]_{4}$, all of these, except for the second one, presented an increase in the load carrying capacity compared to the parent structure itself. Different failure modes were associated to each type,as an example, cohesive failure or CFRP delamination in the 0 patch type and tensile rupture in the 90 patch type . Finally, the minimum equivalent stress was observed in the $[45/\text{-}45]_{8}$ patches.

Campilho et al. [**?**] studied the possible major geometric parameters that have influ-

ence over single and double-lap carbon-fiber composite repaired joints, as well as optimizing them in order to obtain maximum residual strength. The conclusions included the existence of a maximum overlap length above which there is no strength advantage, since the center region becomes unloaded. For SLJ both shear and peel stresses are higher at both interfaces, which justifies why failure will initiate at these locations. Compared to double-lap joints, the peel stresses are higher because of the bending, which may lead to delamination. In terms of stacking sequence, the joint efficiency is higher for the laminates which induce lower strength according to the load direction. The plate's thickness also has a major influence, as its raise decreases the efficiency.Damage initiation was also considered, as it started at the interfaces between the adhesive, parent plate and patch.

Different mechanical properties of bonded repaired composite materials subjected to tensile and compressive loads has been extensively investigated over many years and several analytical and computational models have been developed. However, in terms of bending loads very few studies can be found, specially when specifically applied to single-patch repairs performed on notched composite laminates. This work aims the optimization of a simple repair technique that allows recovery of secondary aircraft structures in locations where little to no preparation is possible, combined with a low cost and brevity. The optimization is developed according to two variables, the patch size and laminate stacking sequence (equal for both the laminate and correspondent patch). Therefore, the present work seeks to add to the previous studies and provide a better understanding of design considerations to have when repairing a structure and associate the flexural, impact and fatigue testing failure modes to each of the variables and to the mechanical properties studied for comparison. A computational model, developed using a finite element model, to validate the values.

Chapter 5

Mechanical Testing

During the 1980's, a huge number of new mechanical test methods were introduced to the composite-materials community, coinciding with the fast development of many new classes of composite materials. The purpose for these developments was to provide the capacity of selecting between the old and new material systems that were becoming available. Nowadays, with the less new methods being introduced, the priority is to reach a consensus on a minimum number of test methods that adequately characterize composite materials and verify their quality in fabricated forms [**?**].

There are two main intentions when mechanically testing a composite material, which are to obtain preliminary properties data for future comparison but also detailed design data. With the constant creation of new materials, its characterization is achieved by mechanical testing and a followed comparison with already existing and fully studied materials, which provides a good qualification and evaluates possible improvements. Aspects as fibers, reinforcing architecture and matrix, including the interface between them, must be considered. Due to the difficulty and high cost of these tests, the development and implementation of standardized tests are essential for proper generation of design data, quality control and product specifications, however, as a permanently evolving field, many recent methods are still not standardized [**?**].

In general, composite is non-homogeneous and anisotropic, which originates the necessity of always considering a basic unity that is the individual lamina to a full understanding of the obtained data after testing.

The mechanical tests can be defined as static or dynamic. This classification defers according to the type of load that is applied to the specimen, specifically, static material properties are obtained from the response of the material to applied loads whose magnitude and direction does not vary with time, whereas dynamic loads present a variation of magnitude or direction as a function of time, possibly having inertial effects. Both these types of loads can be defined as tensile, compressive or shear [**?**].

Along the next sections the different testing methods used in this work will be explained.

5.1 Flexural Test

A flexural test is considered a quasi-static test and induces tensile, compressive and shear stresses simultaneously, becoming popular due to its simplicity aggregated to the preparation and testing of the specimens. This test can sometimes be excluded from composite material properties tests due to the nonuniform stresses to which the specimen is subjected due to the load, as maximum tension at the lower surface, maximum compression at the upper surface and maximum interlaminar shear at the midplane [**?**].

Usually, solid laminates or beams are tested, with an existence of standards for both, as are examples the three-point and four-point bending tests. A three-point bending specimen is loaded at a single point in the center whilst supported near each end, differing from a four-point bending test only by the two centered loads instead of one. When equalizing the bending stresses at the center of the specimen,of these two tests, the same force must be applied at the single loading point as to the double loading, if the two loads are applied at one-quarter of the support span length from each support [**?**].

When talking about three-point loading, the one used for flexural testing in this work, the maximum bending stresses occur at the center of the specimen, decreasing linearly as approaching the support points [**?**].

Laminate flexure specimens are usually loaded and supported by circular cylinders, which induces local stress concentrations, it is important to ensure that the failure happens due to tension or compression at the surface. However, the high ratio between span length and the thickness of the specimen doesn't allow high enough shear stresses in order to fail, for example, by crushing the plate. This is achieved by setting this ratio to 16:1 or greater [**?**].

During a flexural test, the reaction of the specimen to increasing deflection is measured in order to calculate the bending stress-strain curve. The flexure strain is related to the vertical displacement of the specimen (δ) by Equation 5.1, where L is the support span between the two outer points, and w and h are the width and thickness of the specimen, respectively. The three-point bending flexure stress is determined by Equation 5.2, where P is the applied force [**?**].

$$\varepsilon_f = \frac{6\delta h}{L^2} \quad (5.1)$$

$$\sigma_f = \frac{3PL}{2wh^2} \quad (5.2)$$

Flexure tests are often preformed on brittle materials and fiber-polymer composites in order to determine flexural modulus, yield stress and breaking stress, the latter being the most prominent in this work [**?**].

5.2 Impact Test

When a relatively sudden application of an impulsive force is applied to a specific volume of material or structure, it is defined as an impact. However, this definition is ambiguous, leading to multiple and divergent author's interpretations [**?**].

Its effects are widely known, however, it can be quite hard to analyze the phenomenon. It is important establish the relation of the caused effects to the applied forces and the properties of the material, which allows the study and prediction of the outcome of a specific event. The impact can result in a large spectrum of effects, from an elastic result, where the energy is dissipated as heat, propagating internally through the material, to a plastic reaction, causing deformation or even different levels of permanent damage [**?**].

During the study of failure processes, new materials and situations are initially studied through comparison with existing cases, and, being that metals are the main class of materials used in high performance applications, it is the most common point of comparison when starting to study composites. However,this comparison study fails when it comes to the behavior of these two materials, as most metals have a plastic response to the impact, causing a supposed permanent deformation or damage that can be overcome by annealing or reworking the material and structure, which is not possible in polymer matrix composites, that despite presenting an elastic behavior, once the damage is reached, it becomes irreversible [**?**].

When studying a composite material, the study of the impact damage is essential since it is a type of damage that can occur during the life of the structure, resulting in the reduction of its mechanical properties and possibly going unnoticed, being called a barely-visible impact damage (BVID). This study starts by specifying the dynamics of the impact on the composite structure by the foreign impactor and measure not only the contact force but also the response of the structure itself. Secondly, understand the progress of the damage, the failure modes and what factors can affect damage resistance, and then, it is possible to determine the overall effect of impact damage on the mechanical properties of the original structure [**?**].

Specifically , when impacting composite materials, it is expected permanent damage, visible or BVID, penetration or even fragmentation, which implies a change in the structural properties. Contrariwise the response of a metal to the same conditions, which may undergo plastic deformation and still maintain its integrity. This contrast is due to the former's low transverse and interlaminar shear strength, laminar construction and nonexistent plastic deformation [**?**].

When it comes to the characterization of impacts, they can be separated into either low, high or ballistic velocity, however, when looking for specific limits of each category,

it is hard to find a consensual definition between authors.

Low-velocity impacts were defined by Sjöblom and Shivakumar as events that can be treated as quasi-static having a maximum velocity from 1 to 10 m/s and as being dependent of the target and impactor's material properties and stiffness. This definition implies the dynamic structural response of the structure as the main difference between both types of impact,which means, during the stress wave propagation, the response to an high-velocity impact consists of a localized damage, as the impact event is ceased before the stress waves reach the edges of the structure. This is not verified in the other case, as the contact duration allows the full structure to respond to the impact, absorbing elastically more energy [**?**].

Cantwell and Morton followed the generally used test techniques of impact simulation , instrumented falling weight impact testing, to define the maximum velocity of a low- velocity impact as 10 m/s, which largely contrasted with the studies of Abrate, with a defined limit of 100 m/s [**?**].

Liu and Malvern and Joshi and Sun identify the type of impact by the damaged caused on the structure, specially in cases that the damage is the main concern. High-velocity is identified by penetration-induced fibre breakage and low velocity by delamination and matrix cracking [**?**].

Davies and Robinson's definition is based on the through-thickness stress wave, simplyfing the low-velocity impact as not being influenced by it, and favoring the transition to a high-velocity impact. Following this, a cylindrical zone under the impactor is considered to suffer of an uniform strain as the stress wave propagates through the structure, defining the compressive strain as in Equation 5.3. From this, failure strains between 0.5 and 1 %, establishing the transition to stress wave dominated events at 10 to 20 m/s for epoxy composites [**?**].

$$\varepsilon = \frac{\text{impact velocity}}{\text{speed of sound in the material}} \quad (5.3)$$

When talking about low-velocity impact, there are four major failure modes when it comes to impacted composite laminates, matrix mode, where the crack appears parallel to the fibers due to tension, compression or shear, delamination mode, by interlaminar stresses, fiber mode, breakage on the fiber when in tension and buckling when in compression, and finally, penetration, the impactor goes through the structure. By identifying each of these modes, it is possible to evaluate not only information about the impact itself but also the structure's residual strength [**?**].

Matrix damage is the primary failure caused by the transverse low-velocity impact, in the form of matrix cracks and debonding of the fiber and matrix, the first usually is

oriented in parallel planes to the fiber direction in unidirectional layers [**?**].

Delamination follows the matrix crack that goes through the resin-rich area between plies of different orientations, when caused by transverse impact, only occurs in presence of this initial crack, called critical matrix crack, after the threshold has been reached. [**?**] The propagation of delamination, by a constant load, can cause a drastic reduction on the strength and stiffness of the laminates, which combined with the composite laminates lack of reinforcement in the transverse direction and the inherent weakness of their interfaces, justifies the high importance of studying this failure mode in order to establish the relation of the cracks to the stresses caused by the impact and the delamination itself [**?**].

Fiber failure usually occurs in the latter phase of the fracture process and is less studied in the low-velocity impact field, usually occurring in the are under the impactor,where there is a concentration of high stresses and indentation effects, and on the periphery due to high bending stresses. Penetration is a macroscopic mode of failure that follows a critical fiber failure, allowing the impactor to puncture the full thickness of the material [**?**].

When interpreting the impact damage it is relevant to understand that the laminate suffers a stress distribution which goes from compression to tension through its thickness, as a result of the impact-induced flexion. The stacking sequence influences the stiffness of the laminate, therefore has a major effect on the material strength, that in turn defines if the damage initiates on the impacted surface, for stiff laminates, or on the opposite surface, for flexible laminates [**?**].

5.3 Fatigue Test

Fatigue is defined as the deterioration to the structural properties of a material owing to damage caused by fluctuating stresses [**?**]. This becomes relevant in aerospace materials due to the needed capacity of these structures to withstand repeated loading for long periods of time, in the range of 15000 to 20000 flight hours for modern jet engine materials and anywhere from 80000 to 120000 hours for airframe materials. The damage caused by the repeated both mechanical and thermal-induced loading causes a loss in strength leading to potential failure, therefore making use of the fatigue tests allows the measurement with precision of reduction in stiffness and strength of the material and to determine the total number of load cycles to failure [**?**].

Fatigue tests measure the resistance of materials to damage, strength loss and failure under the repeated application of load. These tests are performed by repeated tension-tension, compression-compression, tension-compression and other combinations of cyclic loadings. The fatigue stress is characterized by multiple load waveforms, which shape is

usually sinusoidal. The frequency of the load cycles is low, typically between 1-20 Hz, to avoid the heating of the material, which could affect the results [**?**].

The fatigue cycle has several important stress parameters that can affect the fatigue properties of materials, as maximum fatigue stress, mean fatigue stress, fatigue stress ratio and the stress frequency, all being proportional to the fatigue damage and failure [**?**]. The basic method of determining the fatigue resistance of the material is the fatigue life curve (S-N), as a plot of the maximum fatigue stress, S, against the number of load cycles up to failure of the material, N. The test can be stopped after a specific number of load cycles and then the specimen is loaded in order to measure the residual fatigue strength [**?**].

Fatigue of composites is characterized by a multiplicity of damage types, including cracks in the matrix, debonding between the fibers and matrix, splitting cracks, delamination and broken fibers. The failure modes initiate at different times and present different rates over the fatigue life of the material therefore composites tend to fail progressively due to multiple damage events rather than because of a single crack. At high fatigue stress and short life, the damage is dominated by fiber breakage [**?**].

Chapter 6

Materials, Equipment, Experimental and Numerical Procedures

In this chapter the manufacture process of the specimens, materials and equipment used will be described. The experimental procedures and numerical analyses will be presented and described in detail.

6.1 Sample Manufacture

Along this study two different laminates were used, according to the goal of the present thesis as a study and optimization of different overlap lenghts of adhesively bonded patch repairs in drilled laminate plates , different composite laminates were prepared in the laboratory. The laminates were made from unidirectional carbon Prepreg, TEXIPREG® Hs 160 REM, which properites are shown in 6.1 provided by the company SEAL, Legnano, Italy. The CFRP laminates were prepared by prepreg lay-up, process described in Section 2.4.

Table 6.1: Properties of TEXIPREG® Hs 160 REM [**?**].

Elastic Modulus (MPa)	Poisson's Ratio	Shear Modulus (MPa)
E_1=1.09E5	υ_{12}=0.342	G_{12}=4315
E_2=8819	υ_{13}=0.342	G_{13}=4315
E_3=8819	υ_{23}=0.380	G_{23}=3200

The first laminates, used for the main plates, were made with twelve plies of Prepreg presenting a stacking sequence of $[0,90,0,90,0,90]_S$, while the second type of laminates, as the patches material, used only eight plies of material with a stacking sequence of $[0,90,0,90]_S$. This set up, compressed between two bigger plates, follows multiple steps during the autoclave processing as suggested in the manufacturer recommendations, which are being sealed inside a bag and put in constant vacuum using a pump, using a compressor to define the pressure inside the chamber as 1 bar which makes the temperature rise, with a rate of 2 to 4 ºC/min, up to 100 ºC, followed by an applied pressure of 5 bar and maintaining both pressure and temperature for 150 min, approximately, and finally cooling down to room temperature.

The laminates were made with a planned size of 320 mm $\times$ 320 mm, with an approxi-

mate thickness of 1.8 mm, in order to cut six of the main plates with the single dimension of 150 mm $\times$ 100 mm and multiple square patches, in the thinner laminates with only 1.2 mm of thickness, depending on the chosen dimension of 30, 40 or 60 mm. The samples were cut using a automated diamond saw machine with a constant cooling system, allowing clean edges and a small dimension error. A total of 99 plates, 47 following the same orientation as the laminates that were made and the remaining with the perpendicular direction $[90,0,90,0,90,0]_S$, and 27 patches of each size were cut, according to the defined parameters to be studied.

The specimens were tested as full intact plates, drilled plates, representing the removed fractured area, and repaired plates using the patches, therefore part of the plates were also drilled, creating a centered hole with 20 mm of diameter. Finishing this initial processing of cutting, there were two different types of individual pieces, shown in Figure 6.1.

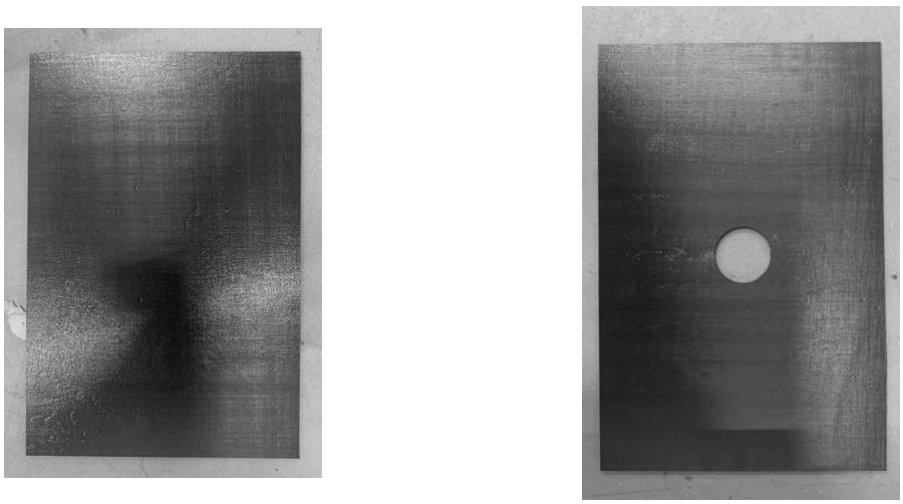

Figure 6.1: Parent and drilled specimens.

Other than the parent and drilled specimens that were ready for testing, the remaining drilled plates were repaired using an adhesively bonded single patch, one-sided. A two part was used structural epoxy adhesive 3M^{TM}Scotch-Weld^{TM}9323 B/A prepared with a weight ratio of 100 to 27 following the manufacturer recommendations, as shown in Appendix A, and mixed with 0.8 g of micro glass beads(diameter of 150μm, approximately). The adjacent faces of both the patches and plates were roughened by sand paper, grit size 240, and cleaned in order to increase the adhesion at the adhesive/composite interface, the adhesive was applied in both surfaces, on an area with the same dimensions as the correspondent patch, and the surfaces were pressed down with weights in order to create a considerable fillet of adhesive around the full thickness of the patch, as uniform as possible throughout the specimens.The thickness of the adhesive was found to be approximately constant and about 0.2 mm. The specimens stayed pressed for about 24 hours and post-cured in an oven at the temperature of 75 ºC for 2 hours, according to the manufacturer recommendations for testings performed at 23 ºC.

Finally, the specimens were marked with a white pen in three positions, working as

guidelines in order to facilitate the placing of the specimens in the bending and fatigue fixture. In Figure 6.2, the repaired specimens geometry is shown, where *d* represents the patch length variable as 30, 40 or 60 mm. The three perspectives of the repaired specimens are shown in Appendix B.

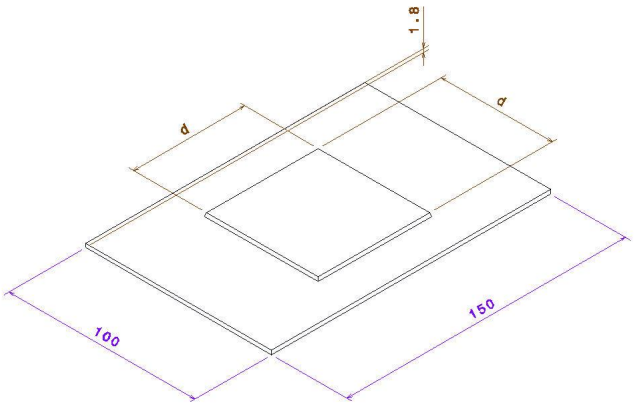

Figure 6.2: Overall geometry of the repaired specimens.

6.2 Equipment

To perform the three-point bending and fatigue test, a fixture, represented in Figure 6.3, was used that allowed the rectangular specimens to be fixed both in the x, y and z axis but free to rotate around the fixed lines along with the vertical displacement applied to central line of the plates. With these requirements, the fixture used consisted of three identical structures, two of them representing the stationary base with a distance of 100 mm between them that pinned both ends of the plate , and the third one, between of the others and in opposite direction, responsible for fixing the center of the specimen and forcing the displacement.

The quasi-static three-point bending tests were performed using a Zwick/Roell tensile testing machine, as shown in Figure 6.4, equipped with a 10 kN load cell and correspondent software to collect and analyze the results.

The low-velocity impact tests were performed using a drop weight impact tower, in-house made, with an impactor that weighed 2.9 kg and had a diameter of 12 mm, as shown in Figure 6.5. The impact energy is generated only by gravity and controlled by adjusting the initial height from where the impactor is dropped, which velocity is measured by an optical sensor, and later, after the first impact with the specimen, stopped by a mechanical claw.

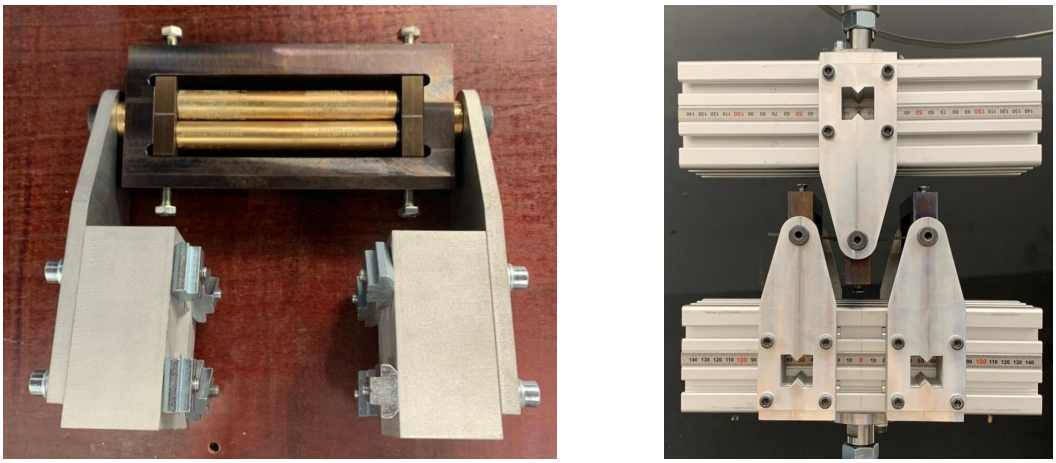

(a) (b)

Figure 6.3: Fixture used for bending and fatigue testing: (a) single fixture; (b) full support structure.

Figure 6.4: Tensile testing machine (Zwick/Roell)

In order to define the desired potential energy to impact the specimens, it is important to acknowledge the losses between the calculated and measured value of velocity needed to achieve a correspondent kinetic energy.

The bending fatigue tests were performed using a fatigue machine MTS 100 kN Elastomer, in which the fixture was attached, resembling the previous bending setup, as shown in the Figure 6.6.

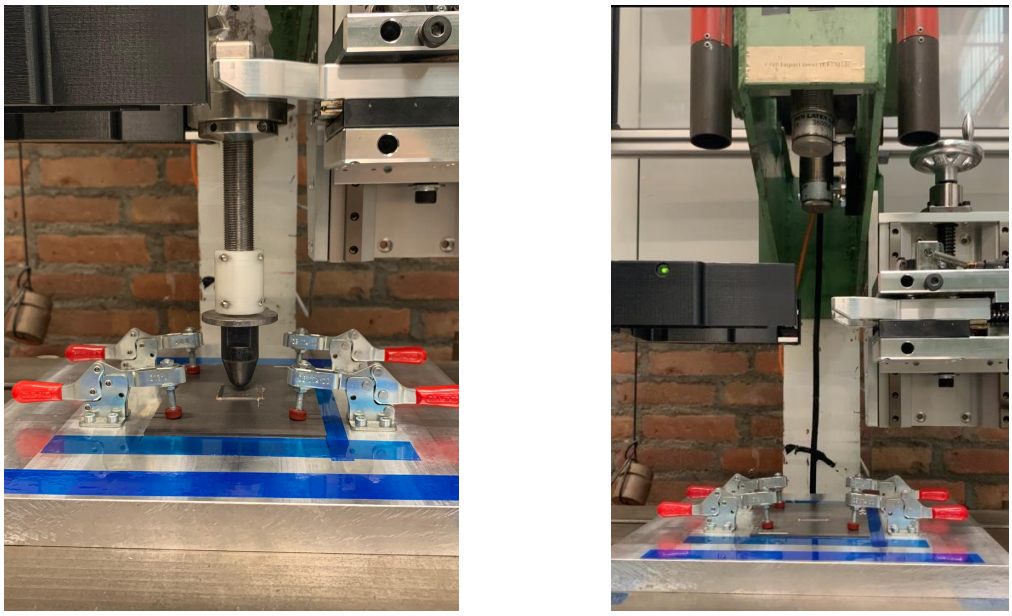

(a) (b)

Figure 6.5: Impact tower: (a) impactor; (b) full structure

Figure 6.6: Example of fatigue machine [**?**].

6.3 Experimental Procedures

The experimental study was performed using the specimens and equipment described previously, and carried at room temperature. Five different types of specimens, as a total of 99 pieces, were tested. The specimens were distributed by the different tests and

categorized according to their geometrical parameters to facilitate the overall process and discussion of results. The specimen is defined by the geometry, experimental test, stacking sequence and patch size. The geometry is classified by parent laminate (I), drilled (H) or repaired (not defined), followed by the experimental test, bending (B), impact (I) and fatigue (F), and finally the combination between stacking sequence (0 or 90) and selected the patch size (30, 40 or 60). Therefore the number of specimens tested for each of the studied types are shown in Table 6.2.

Table 6.2: Number of specimens tested (*- number of specimens tested for each patch size).

Type of specimen	Number of specimens tested
IB-0	4
IB-90	5
HB-0	4
HB-90	5
B-0	4*
B-90	5*
I-0	5*
I-90	5*
F-0	4*
F-90	5*

The low velocity impact tests were the first to be performed, as the tested specimens needed to be tested in bending. The energy of the single impact was previously selected in order to achieve a barely-visible damaged area in the laminate, that was later measured using C-scan technique, but without reaching perforation of the specimen. The offset height of the impactor relatively to the specimen was defined to 500 mm in order to achieve a measured velocity value of around 2.9 m/s which corresponds to a kinetic energy of 12 J, approximately. The samples are centrally clamped to a support in order to have a centered stroke by the impactor.

The three-point bending tests were performed using a displacement rate of 3 mm/min with a maximum span of 22 mm. The test was carried up to a drop of 60% of the load value, where the test stopped automatically, or after verifying a clear failure mode, stopped manually by the user. The displacement of the center line of the sample, in the direction of the applied load during bending, and the correspondent load values collected from the experiment, allow the results to be obtained in the form of force-displacement curves at the center line of each specimen. Therefore, the results will be presented in terms of average maximum load and bending stiffness.

The bending fatigue behavior, at constant deformation, was tested at a stress ratio of approximately 0.33 and a frequency of 3 Hz, in order to avoid heating of the specimens and guarantee that the damage depended only on the load/time and not on the temperature. The value of maximum stress was defined according to 55% of the maximum displacement values before failure, according to the bending tests. When reaching the ultimate failure of the patch repair, the test stops. The maximum displacement values for each specimen type, obtained from quasi-static testing and converted according to the stress ratio, are

specified in Table 6.3.

Table 6.3: Maximum displacement values used for fatigue testing.

Specimen type	Maximum displacement (mm)
0^0 - 30	5.63
0^0 - 40	6.19
0^0 - 60	5.63
90^0 - 30	3.38
90^0 - 40	3.65
90^0 - 60	3.38

6.4 Numerical Model

The numerical analysis was performed in the commercial FEM software ABAQUS to validate the results obtained from the bending tests and assess the effects of the stacking sequence and patch size on the stress distributions. In this analysis, the lamina properties of the layered composite laminates were specified and assigned to the shell geometries of the main piece and patch, including the lamina thickness, material and stacking sequence.

As this analysis aims to verify stiffness values, it was chosen not to simulate the adhesive as its stiffness was considered despicable compared to the ones from the composite structures, specially when it comes to a flexural test. This choice was also made due to the length scale difference between the different parts of the samples. The meshing of the adhesive, with a thickness of 0.2 μm, represented the need of a much smaller mesh, which would be time consuming, and a mesh refinement that could lead to possible lack of compatible nodes.

The dimensions of the samples used in the finite element analyses were the same as the ones used in the experimental study. Quadrilateral and shell elements were used in the mesh of both parts, with an exception of few triangular elements around the notch edges of the drilled plate. For the simulation of all parent laminates, either intact or drilled, 3 mm elements were chosen and after meshing the part, a total of 1650 elements and 1734 nodes were obtained for the intact parts and 1786 elements and 1866 nodes for the drilled ones. These meshes were common for both simulation, individual or after applying the repair to the analysis. For the patches, quadrilateral elements of 1 mm were used and the mesh presented, for the 30, 40 and 60 mm patches, 900, 1600 and 3600 elements and 961, 1681 and 3721 nodes, respectively. The typical mesh for the overall structure is shown in Figure 6.7.

In order to simulate the boundary conditions provided by the fixture in the experimental tests, The loading conditions were simplified as a remote displacement of 200 mm applied to the center line on the base of the main part. With a centered span of 100 mm, at each extremity a boundary condition, the displacement in the y and z direction, and

rotation around x and z axis, were constrained to the initial position, as shown in Figure 6.8 with the representative axis. The bond between main piece and patch was defined as tie between both surfaces.

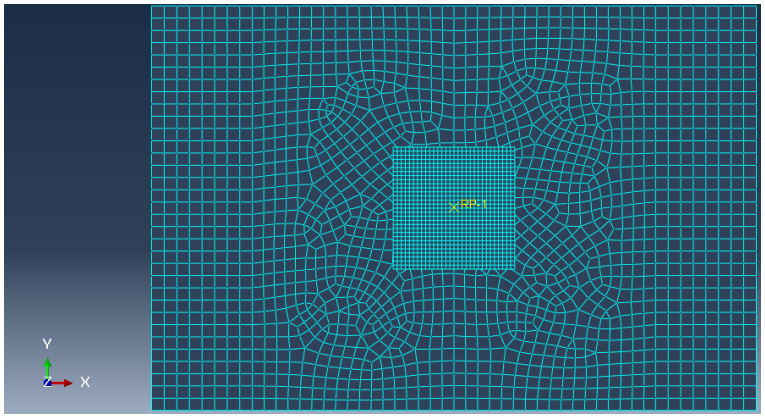

Figure 6.7: Typical mesh of the plate and patch.

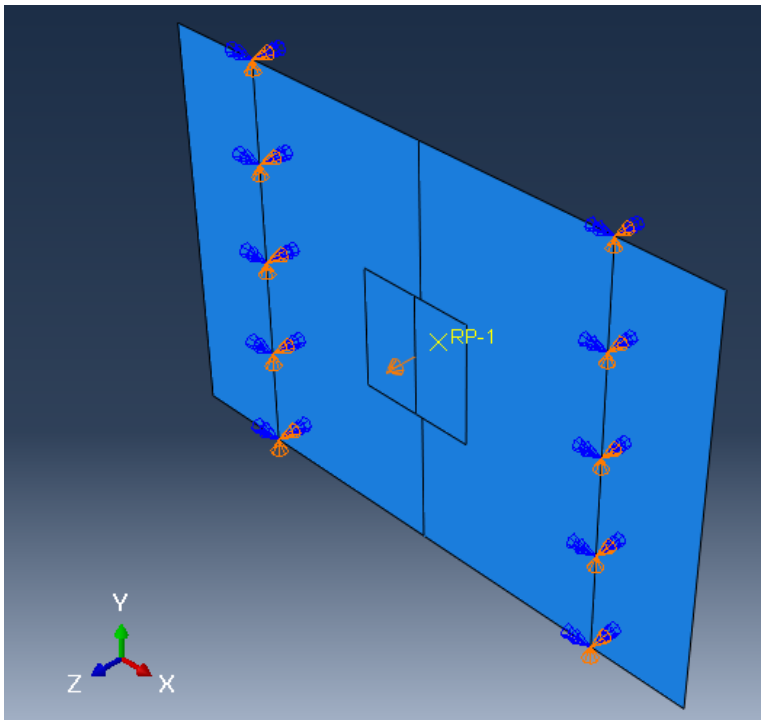

Figure 6.8: Boundary conditions applied to the structure

Chapter 7

Results and Discussions

This chapter presents all results obtained from the experimental tests and respective discussion supported by the open literature. The discussion is divided in four different sections, where, in the first one the effect of drilling the parent plate will be analyzed (experimentally and numerically) in terms of bending stiffness and load. These values will be compared to theoretical stiffness values. The following section assesses the effects of patch size, for specimens with the same stacking sequence (0º and 90º), in terms of impact, where the failure modes will also be evaluated and discussed. Finally, the last section presents the fatigue performance for each stacking sequence and correspondent patch sizes. It should be noted that, during the discussion, the two different types of stacking sequences are mentioned and identified as 0º or 90º which refers to the outermost ply of each one of them.

7.1 Comparison between Parent and Drilled plates

In order to evaluate the effect of a hole in the parent plates, which represents the removed damaged area in the structure, it was necessary to find the theoretical bending stiffness of the parent composite laminates, so a comparison between experimental and theoretical values can be made. This value was calculated according to both stacking sequences and to the material properties of the lamina indicated in Table 6.1. As the plates are assumed to have perfectly bonded layers with a continuous displacement components throughout the thickness and with homogeneous lamina, subjected to transverse and in-plan loadings, it is possible to develop the relations between the external loadings and the displacements. This study was made based on the Classical Lamination Theory (CLT) [**?**, **?**, **?**, **?**]. The parent plates' bending stiffness matrix obtained for each of the stacking sequences are:

$$\{D\}_0 = \begin{bmatrix} 35.05 & 1.480 & 0 \\ 1.480 & 22.76 & 0 \\ 0 & 0 & 2.097 \end{bmatrix} GPa \cdot mm^3$$

$$\{D\}_{90} = \begin{bmatrix} 22.76 & 1.480 & 0 \\ 1.480 & 35.05 & 0 \\ 0 & 0 & 2.097 \end{bmatrix} GPa \cdot mm^3$$

The equations used to calculate these matrices can be consulted in Appendix C. From these matrices it is possible to find the theoretical stiffness of the parent plate, using Equations 7.1-7.2, where L is the span of the plate, w is the width, h the thickness, E the Young's modulus and K the bending stiffness. The theoretical stiffness for each of the stacking sequences is shown in Table 7.1. These values were compared to the simulation stiffness values obtained from the numerical analysis explained in Section 6.4, and the error between both was defined, as they represent a more similar behavior of the same object based on its theoretical model, contrarily to the experimental results that depend on the real behavior of the structure under test with specific errors as measuring errors, material deficiency, handling errors, etc.

$$E = \frac{12}{D_{11}^{-1} h^3} \cdot 10^3 \ (N/mm^2) \quad (7.1)$$

$$K = \frac{4wh^3E}{L^3} \ (N/mm) \quad (7.2)$$

Table 7.1: Comparison between theoretical and numerical bending stiffness.

Stacking sequence	Theoretical Stiffness (N/mm)	Numerical Stiffness (N/mm)	Error (%)
0º	167.83	167.31	0.3
90º	108.84	108.87	0.02

From analyzing the previous table, it is clear that the calculated and the FEA results are in close agreement with each other, being that there is a difference of less than 0.3% in both cases. When comparing values in terms of its stacking sequence, and in agreement to multiple studies developed around its effects [**?**, **?**, **?**], it is clear that the 0º laminates present higher stiffness. This is justified by the dependence of the D matrix on the cubic distance of each lamina from the mid-plane, which means that for same material symmetric laminates, when the orientation of the furthest lamina to the mid-plane is other than 0º, the overall bending stiffness of the laminate will be lower. This change is clearer for the 90º laminate because this ply presents lower lamina stiffness.

The experimental stiffness values were obtained from the load-displacement curves of each quasi-static test. Typical curves are shown in Figure 7.1, as representative curves of the specimens from each type. The comparison between stiffness values can be extended to the experimental values, shown in Table 7.2. The disparity between the two results was expected as for either theoretical or numerical calculations the ideal conditions for

the study are assumed as well as basic assumptions in order to apply certain theories and methods to the specific case, while during the experimental tests there are external conditions that influence the results. It is also important to take into a consideration that this study was developed with a small number of specimens for each type of test, which may also influence the results as a single deviation of data has a huge influence in the bulk of the results, however this was also considered when selecting the specimens to be discussed in this chapter.

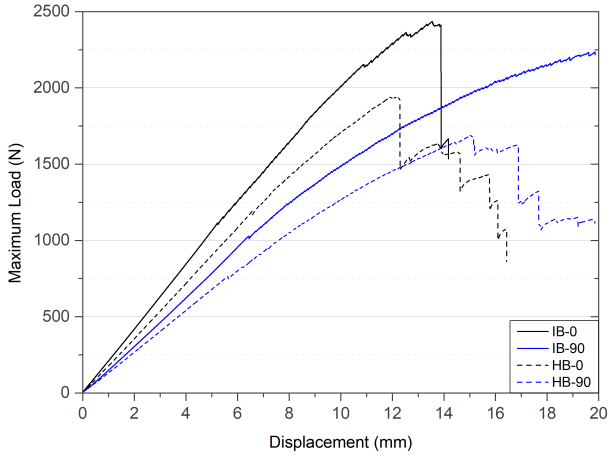

Figure 7.1: Maximum load-Displacement curves for parent and open hole specimens.

Table 7.2: Comparison between theoretical and experimental bending stiffness for parent laminates.

Stacking sequence	Numerical Stiffness (N/mm)	Experimental Stiffness (N/mm)	Error (%)
0^o	167.31	220.08($\pm$ 12.17)	31.54
90^o	108.87	154.43($\pm$ 3.42)	41.85

All curves, in Figure 7.1 present an initial linear region that starts to smoothly deflect, adopting some non-linear behavior, up to the point of maximum load and a ensuing drop of load in the moment of failure, except for the type IB-90 that did not reach a sufficient peak load to fail. The lack of damage failure for these types of specimens is justified by the matrix dominating damage that these parent plates present, which inflicts a low percentage of ductile behavior to the structure, contrarily to the 0^o specimens, as their damage is fiber dominated [**?**]. Considering the specimens with 0^o orientation, in both conditions, the curve after failure is characterized by a zigzag effect that identify a failure mode of fiber breakage, due to the compression in the upper side of the plate, followed by consequent delamination, which is in good agreement with the open literature [**?**, **?**, **?**, **?**]. This also happens in the HB-90 specimens and is justified by matrix cracking.

In the finite element analysis, for the types IB-0/90 and HB-0/90, a displacement of 1 mm was applied to the center line of the plates. By this analysis, the graph of force-displacement (P-Δx) at the center line was drawn and the respective stiffness was compared to the average one obtained from the experiments. The obtained results are reported in Table 7.3 and respective decrease of stiffness from parent to drilled plates.

Table 7.3: Comparison of the effect of open hole in the numerical and theoretical stiffness, and respective decrease.

Stiffness (N/mm)	IB-0	HB-0	Decrease (%)	IB-90	HB-90	Decrease (%)
Numerical	167.31	145.74	12.89	108.87	95.59	12.20
Experimental	220.08	187.59	14.76	154.43	130.99	15.18

From the previous experimental values, it is possible to establish the percentage of stiffness that is lost for specimens with an open hole. The notched plates' stiffness is, approximately, 85% of the parent plates' value, for both orientations. This is an important value to have into consideration as it is relevant to understand if, and how much, the repair will be beneficial to the overall structure.

Similar to study developed for the stiffness, when talking about the effects of open hole specimens, the maximum load comparison is made, in order to discuss the influence of the stacking sequence of the specimens on the maximum load, as shown in Table 7.4.

Table 7.4: Comparison of maximum load between 0º and 90º intact specimens.

Stacking sequence	Maximum Load (N)
0º	2480.52($\pm$ 119.17)
90º	2138.00($\pm$ 57.08)

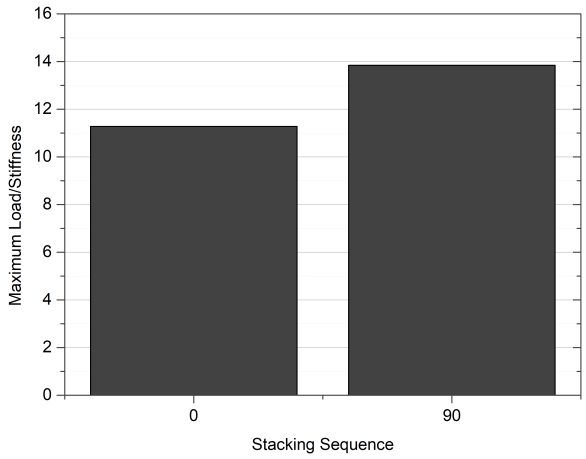

Figure 7.2: Comparison of normalized maximum load for both orientation specimens.

Comparing the load values for the two specimen types, it is noticed that the 0º plates have more strength (approximately 16% more resistance) than the 90º, however, it becomes relevant to consider the normalized load value, i.e, the load is divided by the correspondent stiffness and the obtained value is the one to be considered. This is because the load is dependent of the materials stiffness and is of greatest interest to exclude this dependence as the stiffness was already studied. The comparison of the normalized maximum load is shown in Figure 7.2. According to this data, it is possible to affirm that the previous values of maximum load and its proportions are highly dependent on the stiffness of the laminate itself. Contrarily to the previous tendency, the normalized maximum load is 2.57% higher for the 90º orientation, which means that these specimens can han-

dle more deformation compared to 0º specimens, which is in concordance to the analysis of the curves made previously.

After knowing the properties for the parent plates, it is important to evaluate the effect of the hole on the overall laminate plate. For the purpose of evaluating this effect, the study of the notch sensitivity of the structure to notches or drilled holes. In composite laminates there is a significant reduction in the strength compared to the same un-notched structure.

To assess the notch sensitivity for the composite plates relative to the hole diameter and width ratio, the ratio between the notched and un-notched strengths is calculated. Both limits representing the notch sensitivity and insensitivity are traced [**?**]. These plots are traced considering the behavior of ductile and brittle materials, respectively.

The equations used to calculate these responses in order to the normalized strength are Equation 7.3 for the notch insensitive and Equation 7.4 for the notch sensitive, where $K_T = 2 + [1 - (D/W)]^3$ and (σ_n) is the notched strength, (σ_{un}) the un-notched strength, (D) the hole diameter and (W) the specimen width [**?**].

$$\sigma_n/\sigma_{un} = 1 - (D/W) \quad (7.3)$$

$$\sigma_n/\sigma_{un} = [-(D/W)]\,/K_T \quad (7.4)$$

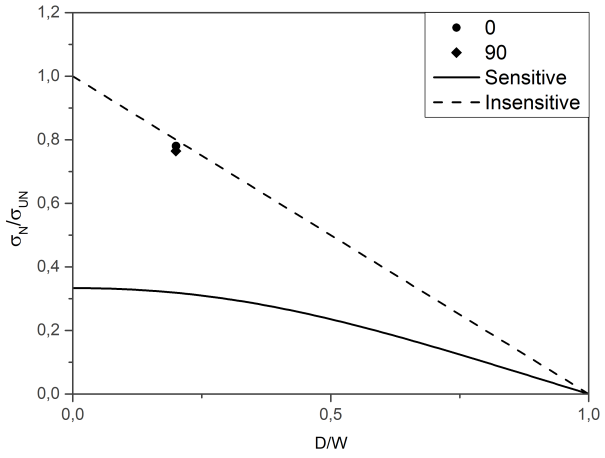

Figure 7.3: Notch sensitivity.

It is possible to observe in Figure 7.3 that the composite falls between the two curves, for both orientations, however, the data is near the top curve, which suggest that the composites have the capacity of load redistribution around the hole. This redistribution is verified for this specific normalized hole diameter, however it can be limited depending on the data tendencies for different D/W ratios. Furthermore, this is dependent on the type of load that is being studied. The flexure behavior of these laminates did not demon-

strate a significant notch sensitivity for this specific D/W, which may not be the case when the loading conditions are different, as for tensile or compressive loadings [**?**,**?**].

From this point on it is important to evaluate the effect of extracting the damage from the original structure. The laminate is considered sensitive to this notch dimensions, which leads to the need of understanding how redistribution of stress around this area can influence the integrity of the structure. In Figure 7.4, the average maximum load data is presented in order to make a comparison between parent and open hole samples.

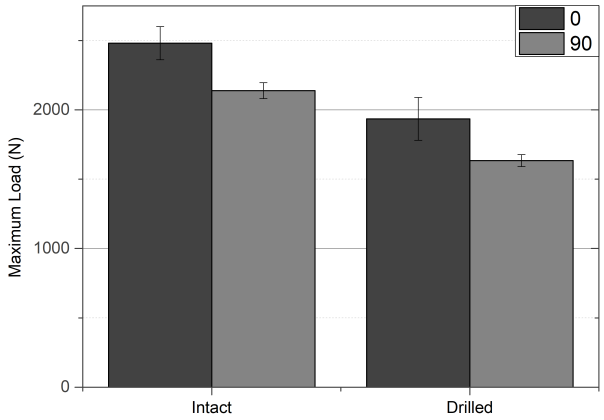

Figure 7.4: Maximum Load for parent and notched specimens.

The load that the open hole specimens can endure, relatively to the maximum loads of the type IB specimens, are, approximately, 78% for the HB-0 and 76% for the HB-90. The variation of maximum load between orientations is related to the stiffness influence in the specimens. Specimens with higher stiffness, endure higher loads in order to achieve the same displacement, for that reason the average maximum load must be normalized in order to compare the maximum stress that each specimen type can endure.

Relatively to the normalized maximum load comparison, the load that the open hole specimens can endure before verifying failure as shown in Figure 7.5 , relatively to the normalized maximum loads of the type IB specimens, are, approximately, 92% for the HB-0 and 90% for the HB-90.

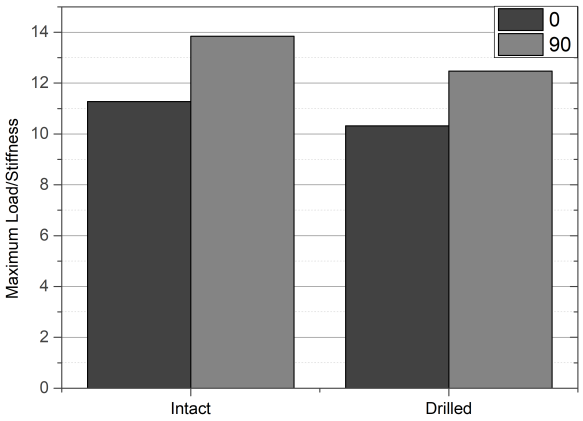

Figure 7.5: Normalized maximum load comparison for parent and drilled specimens.

7.2 Effect of patch size

In this section, the repaired specimens were studied in order to understand the effects of overlap length of the patch on the mechanical properties of a structure. The results will be presented in two subsections, one for each stacking sequence. The effectiveness of the patch overlap length was studied for patch lengths of 30, 40 and 60 mm, to understand their relation to mechanical properties, as bending stiffness and load.

7.2.1 0° Specimens

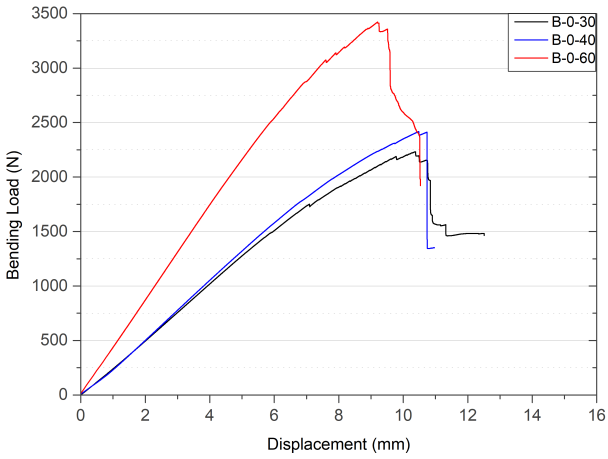

Figure 7.6: Load - Displacement curves for repaired specimens.

The repaired samples were tested in flexural mode and in Figure 7.6 the load-displacement representative curves of the repaired and impacted specimens are presented.

As the specimens present the same parent laminate configuration and the thickness of the patches is also the same, the stiffness variation between sample types is due to the change in overlap length. As it is possible to verify, with the increase of overlap length, the stiffness also increases. This is due to the strengthening of the overall structure by adding more material. These experimental stiffness values are compared to the numerical in Table 7.5.

Table 7.5: Comparison of numerical and experimental stiffness for different patch sizes.

Specimen Type	Numerical Stiffness (N/mm)	Experimental Stiffness (N/mm)	Error (%)
B-0-30	224,14	255,51 (± 13.25)	14.00
B-0-40	282,45	271,98 (± 9.16)	3.71
B-0-60	463,02	429,56 (± 21.47)	7.23

Comparing the previous values, it is possible to establish the increase of the stiffness between notched samples and the repaired ones. For each of the patch repair, the stiffness has an increase of 36.21% for the 30 patch,44.99 % for the 40 and 128.99% for the 60. However adding material also represents an addition of the cost. Even though the increase of the stiffness represents an increase of the maximum load of the structure, this is something that only happens up to a certain point, as according to the literature [**?**, **?**, **?**]. The load is carried by the adhesive at the ends of the bonded length, with the increase of the overlap length, this load transfer eventually reach a constant length, stopping the increase of the joint strength.

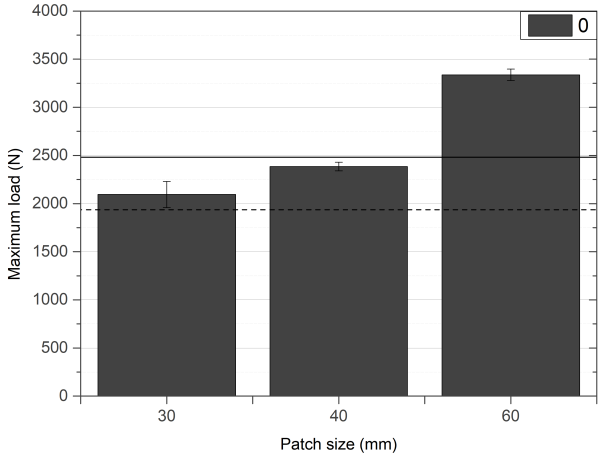

Figure 7.7: Maximum load comparison for each patch size.

Relatively to the maximum load for each of the overlap lengths, presented in Figure 7.7, for the three different sizes tested in this study, the increase of the maximum load is proportional to the increase of the length. In comparison to the notched plates, there was an increase of 8.27%, 23.23% and 72.48%, respectively to 30, 40 and 60 mm. For this reason, at least up to the maximum overlap length considered, the only repair that is shown to be effective is the 60 mm patch, with an improvement in the load carrying capacity of 34.56%, which shows that this on-site repair method using this specific patch

size was effective in restoring and surpassing the unnotched strength. The other patches were not able to restore the load-carrying capacity of the parent plate.

Residual Bending Properties

The single patch repaired laminates with different overlap lengths were subjected to impact tests, with an energy of 12 J, in order to promote BVD. Figure 7.8 shows typical load versus time curves, which are representative of all curves obtained for the studied conditions, and they are in good agreement with the literature [**?**, **?**, **?**, **?**, **?**, **?**, **?**].

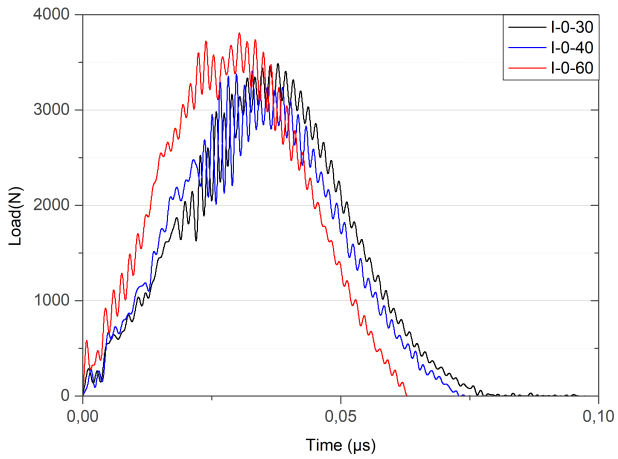

Figure 7.8: Load-time curves for each patch size.

It is possible to observe that the load increases up to a maximum value (Pmax), followed by a drop correspondent to the impactor rebound. These curves (load versus time) contain oscillations as consequence of the vibrations promoted by the samples [**?**, **?**]. On the other hand, the impact energy was not high enough to infiltrate full penetration, as planned, because the impactor sticks into specimens and rebounds always [**?**]. From these curves we can also validate the effect of the patch size on the stiffness value of the specimens, as the steeper the slope of each curve, the higher its stiffness will be. In terms of average values, Table 7.6 shows the maximum load obtained for each patch length.

Table 7.6: Average maximum load values for each patch size.

Specimens	Maximum Load(N)
I-0-30	3479.82 (± 52.6)
I-0-40	3451 (± 126.40)
I-0-60	3855.50 (± 150.57)

Samples repaired with patch lengths of 30 and 40 mm present similar average maximum loads, while for 60 mm the maximum load is around 11.3% higher that the value obtained for the previous configurations.

From a simple observation of the impacted patches, as shown in Figure 7.9, it is possible to identify the type of damage and depth as the color scale refers to the bottom of the parent laminate (0) to the top of the patch (t max). In the 0º orientation, the impact location is visible, surrounded by fiber breakage. From this circular area out, and as the propagation of the impact load is made through the lengths of the 0º external fibers, the visible damage initiates as extensive cracking aligned with the fibers followed by matrix cracking, which is justified, according to the literature, by shearing in the following 90º layers [**?**]. From a visual observation, it is also possible to affirm that the larger the patch size, the less visible damage is verified, as it represents the same impact load applied to a stiffer structure.

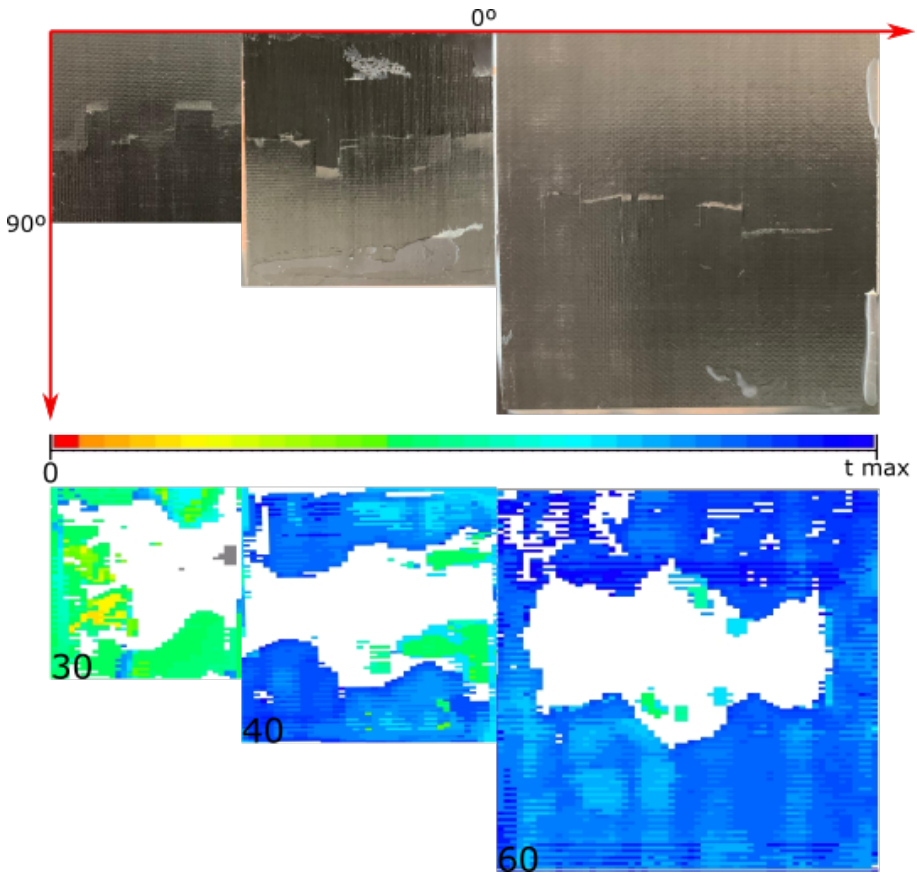

Figure 7.9: Representative impact damage for each patch size: visual and c-scan observations.

Beyond the visual evaluation of the impact damage in the patch, the same specimens were analyzed through a C-scan (pulse-echo mode) in order to evaluate the extent of the barely-visible damage. The delamination, observed in the white areas, presents a circular central area correspondent to the initial area affected by the impactor, where there is a higher stress concentration, and grows in both directions of the patch. This damage pattern shows the damage mechanism caused by the interaction between matrix cracking and delamination. Finally, comparing the dimension of the damage for each of the patch sizes, the damaged area gets close to the patch edges, except for the bigger sized patch. For the 30 mm patch, the damaged area is approximately 38% of the overall area of the patch, while for the 40 mm patch, the affected are is around 43%, and finally, for the 60

mm patch the damaged area is only 22% of the total area of the patch. This difference can have influence in the behavior of the specimens when tested in flexure as the closer the damage is to the patch edges, highest stress concentrations will form in this areas and therefore the faster these specimens will reach their failure point.

Static tests were performed to obtain the residual flexural strength. Three typical load-displacement curves are plotted in Figure 7.10. These tests were performed in order to understand the behavior and change of the mechanical properties of damaged structures and evaluate the efficiency of the repair in that situation. The plots show, for all geometries, an initial linear region followed by some non-linearity up to the maximum load, and a significant drop of the stress after peak stress was reached.

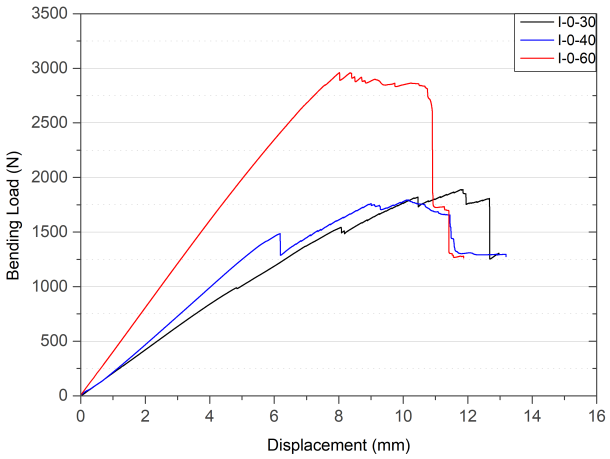

Figure 7.10: Load-Displacement curves for repaired specimens.

The mechanism of damage is the fracture of the fibers, in compression, with delamination in the patch laminate. Probably the propagation of delaminations is responsibly for zigzag aspect of the curve. Figure 7.11 presents the average values obtained from three point static bending test.

As it is possible to observe from Figure 7.11, for all patch sizes, the stiffness of the specimens has a reduction of 6%, 4% and 16% compared to the repaired specimens, which is due to matrix cracking damage [**?**].

Finally, when comparing the maximum load values between repaired and impacted samples, it is possible to state that when a specimen is impacted, the load that it will be able to carry will be less, due to the already existing damage in the patch and consequent residual stiffness. Comparing the impacted specimens, as a structure damage after repair, to the simply repaired specimens, is shown in Figure 7.12.

When compared to the notched specimens, for the 30 and 40 mm patches, there's a reduction of the maximum load, of 7% and 5% approximately. This is also verified when

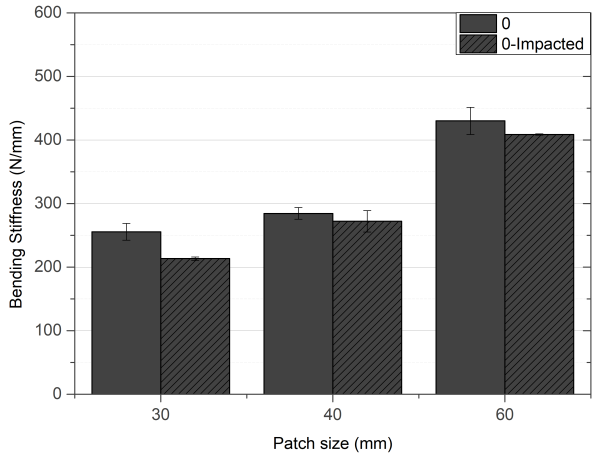

Figure 7.11: Repaired versus Impacted specimens' bending stiffness.

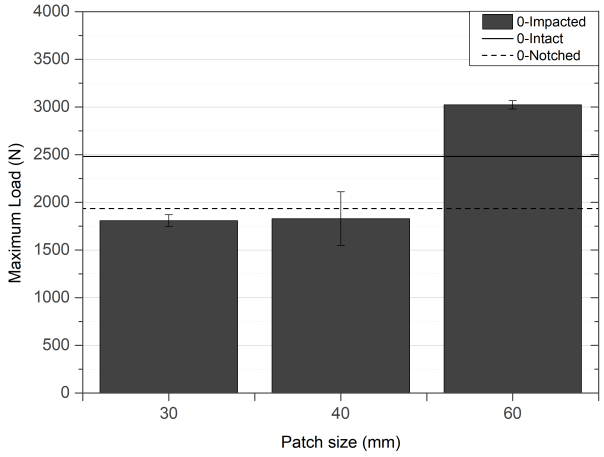

Figure 7.12: Impacted specimens' maximum load comparison with intact and notched specimens.

comparing to the intact specimens, with decreases of 27% and 26%, which indicates that these patch repairs, after damaged, have no sufficient residual strength to keep the integrity of the structure. However, for this specific orientation, the performance of the 60 patch stands out as the only repair that, even after being damaged, is able to carry higher loads than the parent and the unrepaired samples, which justifies the repair of the notched structure and assures that, when eventually damaged by repair, it will keep its resistance above the one of the drilled specimens, and even the intact ones. The samples I-0-60 are able to keep a maximum load 56% higher than the one endured by the damaged structure. The damage described previously also validates these results, as the two smaller patches, with larger damages, fail at similar loads due to the high concentrations of stress that are present in the patch edges.

The failure mechanisms provide information about the efficiency and performance of both the patch size and adhesive bonding. For that reason, it is necessary to examine how

the failure modes change for the different stacking sequences and patch size. The tested specimens were cut at the middle in order to evaluate the damage in the patch. The failure mode verified in the experimental tests, for this stacking sequence, was delamination of the patch, shown in Figure 7.13 and Figure 7.14, verified between different plies depending on the overlap length.For these specific tests, the failure surfaces did not present any adhesive layer trace in any of the adherend or patch, which means no cohesive failure occurred for these types of samples, therefore its is possible to claim that the adhesive does not represent the weak link in the repaired laminates. In the impacted specimen, it is possible to see the area affected by the impact, with a similar pattern to the one in Figure 7.9, where we can verify matrix cracking.

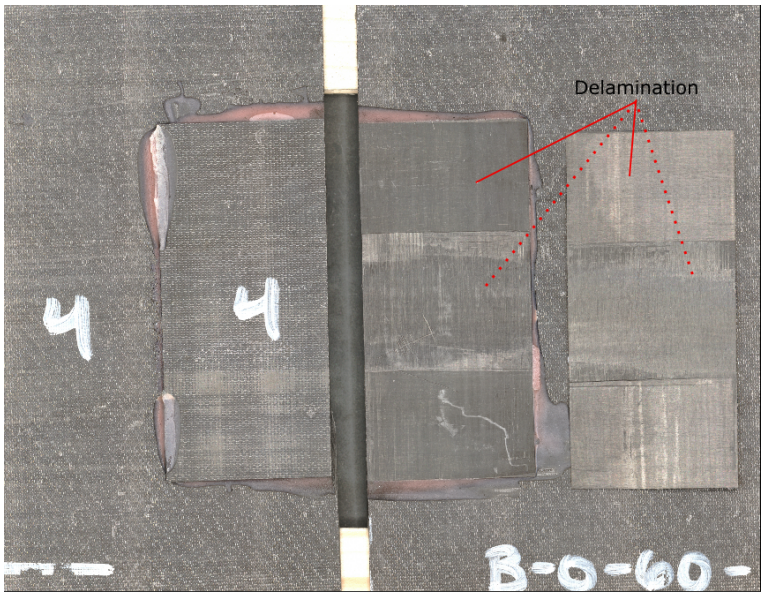

Figure 7.13: Failure in repaired specimen

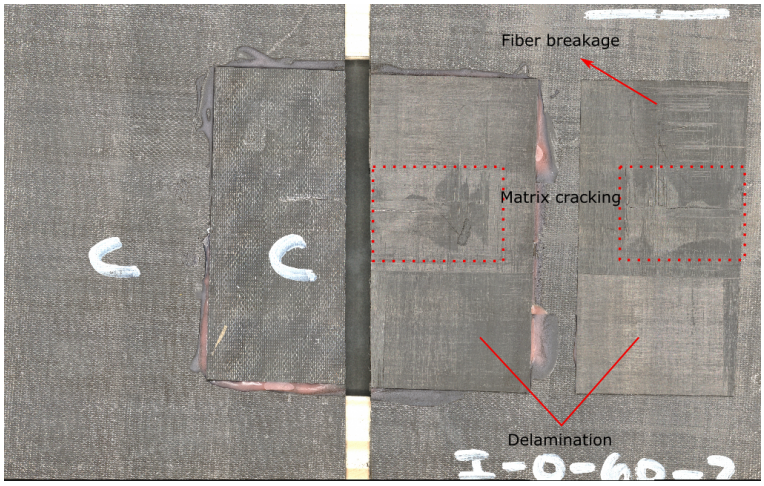

Figure 7.14: Failure in impacted specimen

7.2.2 90º Specimens

On the other hand, within the 90º orientation specimens, the representative load-displacement curves of the repaired specimens are shown in Figure 7.15. From these curves, the experimental stiffness values were obtained and compared to the numerical data, in Table 7.7.

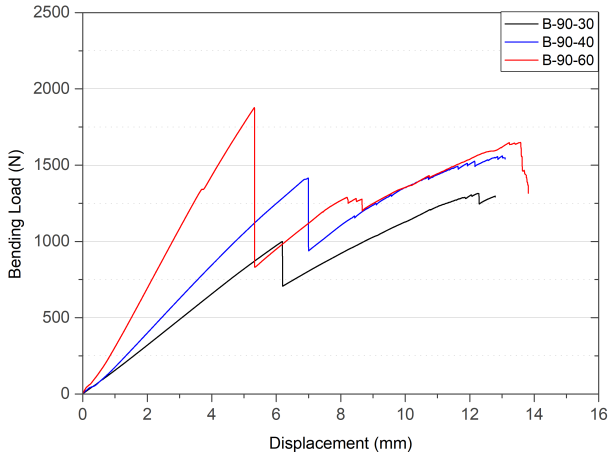

Figure 7.15: Load-Displacement curves for repaired specimens.

The variable that influences the values is the increase of the overlap length of the patches that is shown to be proportional to the increase of stiffness of the samples.

Table 7.7: Comparison of numerical and experimental stiffness for different patch sizes.

Specimen Type	Numerical Stiffness (N/mm)	Experimental Stiffness (N/mm)	Error (%)
B-90-30	160.76	169.12 (± 7.40)	5.20
B-90-40	212.81	222.66 (± 11.93)	4.63
B-90-60	390.64	362.28 (± 15.05)	7.26

According to the table, and considering the standard deviation of the experimental values, the numerical and experimental stiffness values are in close agreement. These repairs also present an increase of stiffness when compared to the drilled specimens, as for each patch size, the stiffness of the samples increased in 29.11%, 69.98% and 176.57%, for 30,40 and 60 mm respectively. These values give a prediction of an improvement in the strength of the specimens, as it is the goal of the repair. However which one of the geometries is shown to be the ideal solution will depend on the maximum load comparison but also on the residual strength of the samples after being impacted. This is similar to the previous study of the 0º specimens, as the increase of the maximum load is proportional to the stiffness, but contrarily to it, the load that the structure can endure stagnates after a specific patch length.

The maximum load, shown in Figure 7.16, and as expected from the previous study, is proportional to the the patch size. However, when comparing the data to the load of

the 90º notched specimens, only the B-90-60 specimens present an improvement of the maximum load that the samples can endure before failing, with an increase of 21.72%, but still does not reach the load carrying capacity of the parent structure, as it is the goal of any repair. Other than these, the other patch sizes have the opposite effect, with a decrease of 40.58% for the 30 patch and 18.30% for the 40. This is due to the fact that, for these two patch sizes, the increase of stiffness was not sufficient in order to improve the resistance of the structure up to the parent laminate resistance, which means that the load-carrying capacity of the damaged structure was not restored neither improved. For this reason, none of these repairs can be considered as an ideal patch repair geometry for this specimen's configuration.

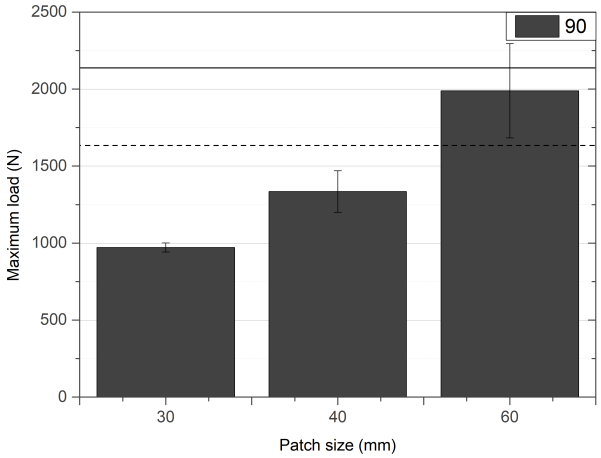

Figure 7.16: Maximum load comparison for each patch size.

Residual Bending Properties

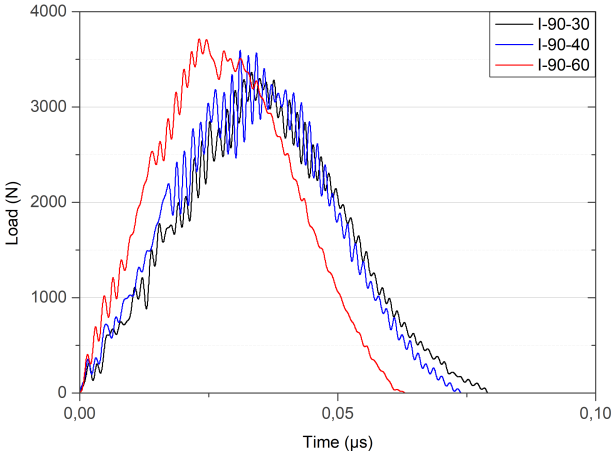

Figure 7.17: Load-time curves for each patch size.

Subjected to impact tests, with the energy of 12 J, the patch repaired laminates suffer

BVD, without penetration. From this tests, Load-Time curves are obtained, in Figure 7.17. The representative curves are in agreement with the literature. From these curves, the maximum load values for each patch size was obtained and shown in Table 7.8.

Table 7.8: Average maximum load values for each patch size.

Specimens	Maximum Load(N)
I-90-30	3361.08 (± 93.16)
I-90-40	3564.68 (± 184.94)
I-90-60	3719.60 (± 225.75)

The average maximum load values present a regular increase between patch length, being proportional to their growth.

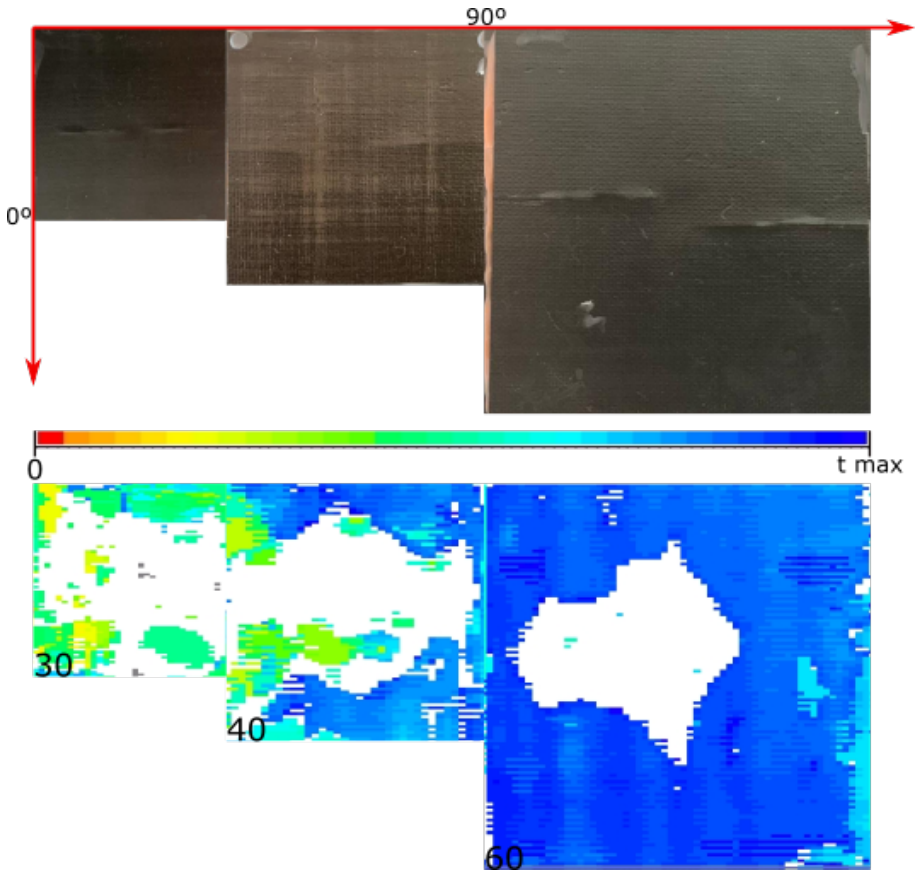

Figure 7.18: Representative impact damage for each patch size: visual and c-scan observations.

When studying the non-perforating impact effects in the repaired specimens, it is possible to visually analyze the damage and the consequences that they suffered. In Figure 7.18, it is possible to establish a comparison between the visible damage that each of the patches, within the 90º orientation, suffered. Common to any of them, the center of the patch, were the impactor hit the sample, shows no visible damage and from this circular region, a damage is verified in both directions. This damage is considered to be fiber breakage, possibly in the second ply of the patch, within the 0º fibers. This damage is expected to be associated with matrix cracking in the interior of the laminate. The color scale is defined from the bottom of the parent laminate (0) to the top of the patch, where the thickness is maximum (t max).

For a better understanding of the damage, the scan images help to locate and evaluate the BVD in the patches. With the 90º external fibers positioned horizontally, it is noticeable that in the two smaller patches the impact caused internal damage in most of the laminate, as, for example, in the 30 mm patch, beyond the delamination that reaches the edges of the patch, the overall laminate presents fiber breakage and matrix cracking all over and in different plies of the laminate, according to the different colors. Contrarily to this, the 60 mm patch shows the centered delamination that propagates through the thickness of the patch, however it does not propagate as hardly to the periphery of the patch which means that in the areas of higher stress concentrations, the structure is less damaged. The damaged area percentage is very similar for both the 30 and 40 mm patches, as the damage covers around 48 to 50% of the overall area of each patch, however for the 60 mm patch this relative area is largely less critical, as only 13.75% of its area is affected, which justifies why the load-carrying capacity is less affected.

Finally, the residual flexural strength was tested in quasi-static modes and the load-displacement curves were plotted in Figure 7.19. The curves are in agreement with the literature, as in the previous similar study, with the same damage mechanisms that are matrix cracking and delamination that slowly propagates up to ultimate patch failure by delamination of the outermost ply of the parent laminate.

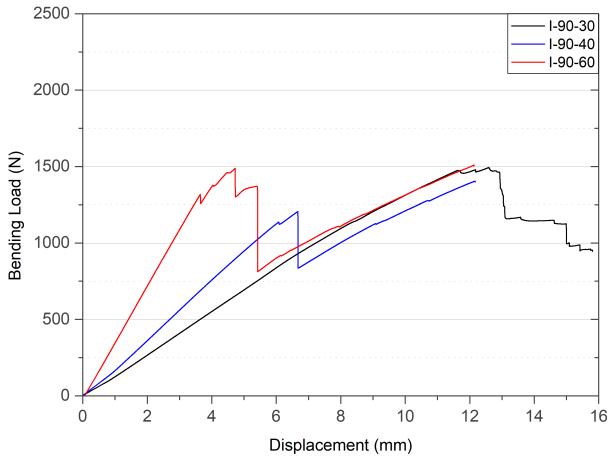

Figure 7.19: Load-Displacement curves for impacted specimens.

Furthermore, after the impact and verifying its effects on the structure, their residual strength is evaluated according to the bending tests' data, in Figure 7.20. As expected, due to the damage in the two smaller patches, the impact leads the structure to a reduction on the stiffness of the samples, with a decrease of 13% and 12% for the 30 and 40 patches, respectively. The stiffness of the repaired and impacted 60-patch specimens remained the same, which can happen because of the small sample of specimens that were studied comparatively to the standard deviation that was obtained, but also because the damage observed in them is less critical compared to the rest, when subjected to the bending load.

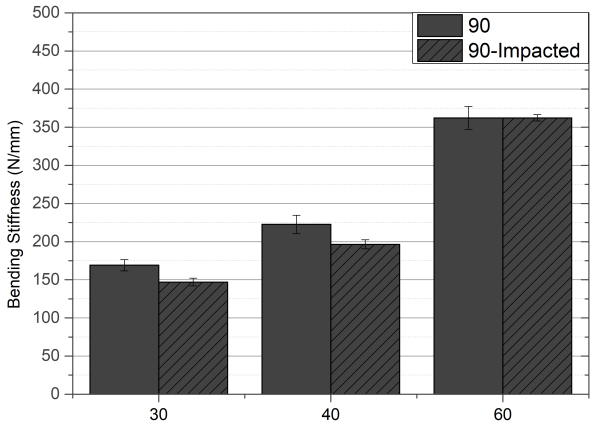

Figure 7.20: Repaired versus Impacted specimens' bending stiffness.

Finally, the maximum load is expected to drop after the repaired specimens suffer any type of damage due to the impact. Knowing that the patch repairs of this stacking sequences were never able to restore the original load of the parent laminate only the comparison between these results and the stiffness of the open hole specimens was made. Each patch size had a decrease of the maximum load, such that all presented lower load-carrying capacities than the notched ones, which means that in case of damage in the patch, the impacted 90º structure degrades to a point of a residual strength lower than the already damaged specimen (notched plate). The impacted specimens presented a decrease of maximum loads of 42.25% for the 30 mm, 31.52% for the 40 mm and 4.66% for the 60 mm patches.

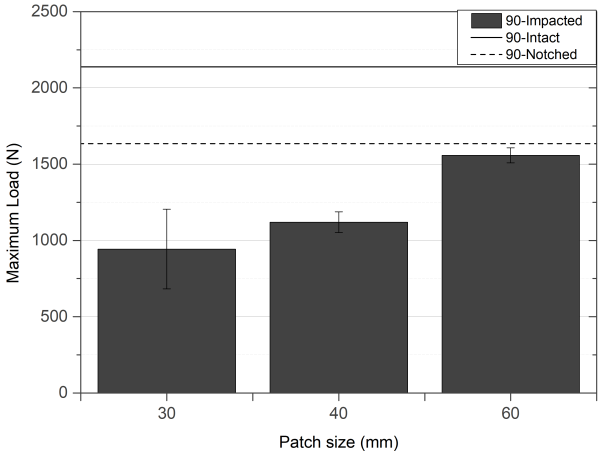

Figure 7.21: Impacted specimens' maximum load comparison with intact and notched specimens.

The failure mechanism can be observed in Figures 7.22 and 7.23, where the specimens are cut in the middle. In these images it is possible to observe that the impact has influence in the failure mechanism of the specimens, as it is easy to see in the center of the

patch were the impactor hit. Similarly to the previous section, no cohesive failure was captured, proving that all failure happened in the composite laminates, in the first plies of the main plate for this stacking sequence. As the patch remains intact, it is not possible to differentiate the area affected by the impact.

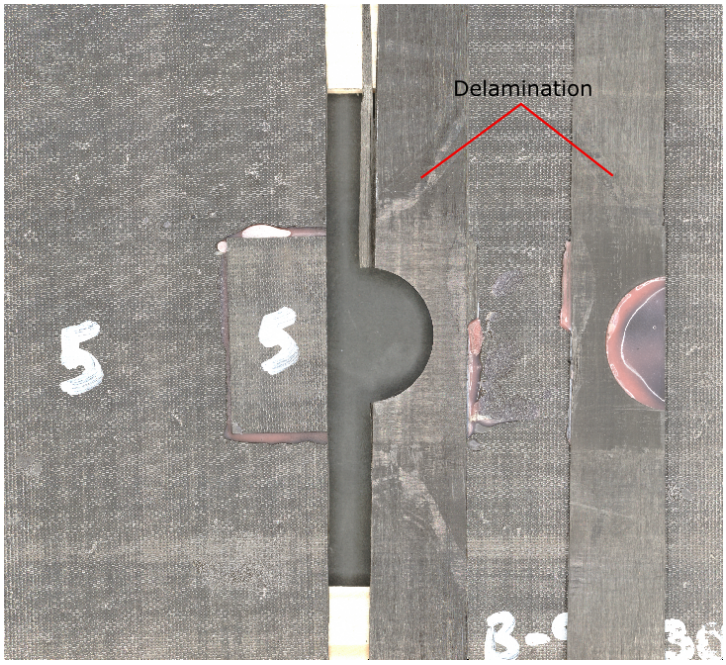

Figure 7.22: Failure in repaired specimen

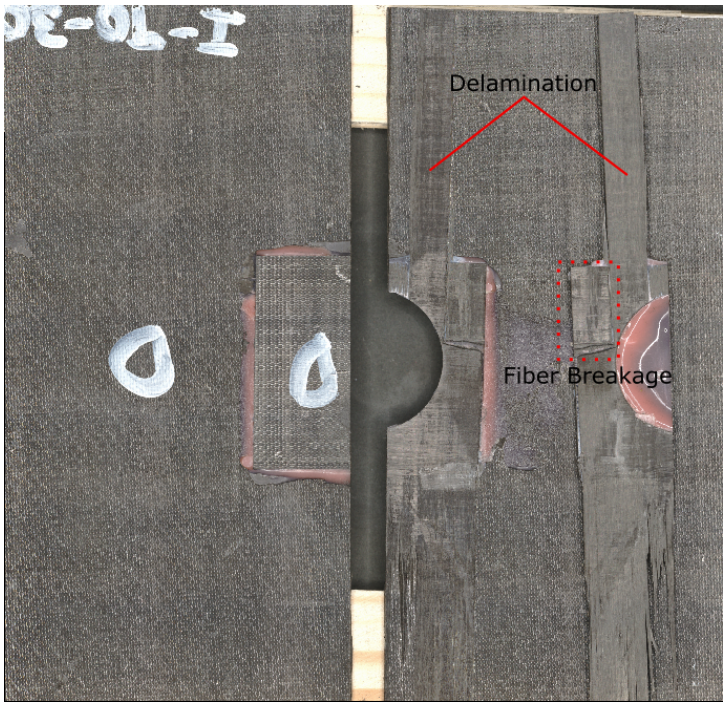

Figure 7.23: Failure in impacted specimen

7.3 Fatigue

The three-point bending fatigue tests were performed considering a specific displacement, as referred previously, where each type of specimens had a specific maximum displacement that corresponded to 75% of their displacement correspondent to the maximum load, obtained from the quasi-static three-point bending tests. The fatigue tests were performed up to the patch ultimate failure, in order to analyze the fatigue behavior of the full samples, and stopped after verifying that the patch was no longer enduring any fatigue effects (only the parent laminate).

The fatigue properties of materials are usually characterized by the S-N curves, where S is the stress level and N is the number of cycles to failure. However, the stress level is dependent on the cross-sectional area, which is not constant for the specimens in question. Therefore, for the sake of comparison, the curve is presented as a function of the normalized force, by F/F0, which is the ratio between the force and the initial force, and the number of cycles, in order to have clearer observation and interpretation of the data. In Figure 7.24, representative curves of each patch size specimens are shown.

According to the data, the curves can be divided into four different sections, with different slopes, which correspond to different damage mechanism types [**?**,**?**]. Initially, the slope of the curve is very steep due to the fast decrease of the load and degradation of stiffness that the specimen suffers. This section of the curve corresponds to the damage initiation, as the matrix cracks start to appear, as the main failure mode expected from the bending tests. From this point on, the curve becomes relatively flat, attributed to a slower degradation of the specimen, which is the longest stage with continuous but small damages in the fiber/matrix interface and small amount of fiber breakage, and initiation of the delamination. Finally, in the last stage, there is a sudden drop in the load, where the interface debonding between fiber and matrix occurs, and the delamination in the specimen gets to the point of critical damage leading to failure. [**?**,**?**,**?**,**?**,**?**]. From the point of ultimate failure, the structure strength is fully supported by only the mother plate, which in this specific study, loses relevance to the discussion, and is represented as dashed curves.

For both stacking sequences the fatigue behavior is similar, however when talking about the ultimate failure damage, the delamination occurs in different regions of the specimens. For the 90º specimens, the partial delamination occurs between the first and second plies of the parent laminate, parallel to the patch width and reaching a maximum length similar to the patch length. On the other hand, the 0º specimens suffer delamination in the patch itself, propagating up to the middle part of the patch, limited by the contact of the fixture pins to the samples in this area. The reason for these types of damage verified are the high concentration of peel stresses in the edges of the patch that lead to the initiation of matrix cracks and lead the structure to a critical state that causes the ultimate failure.

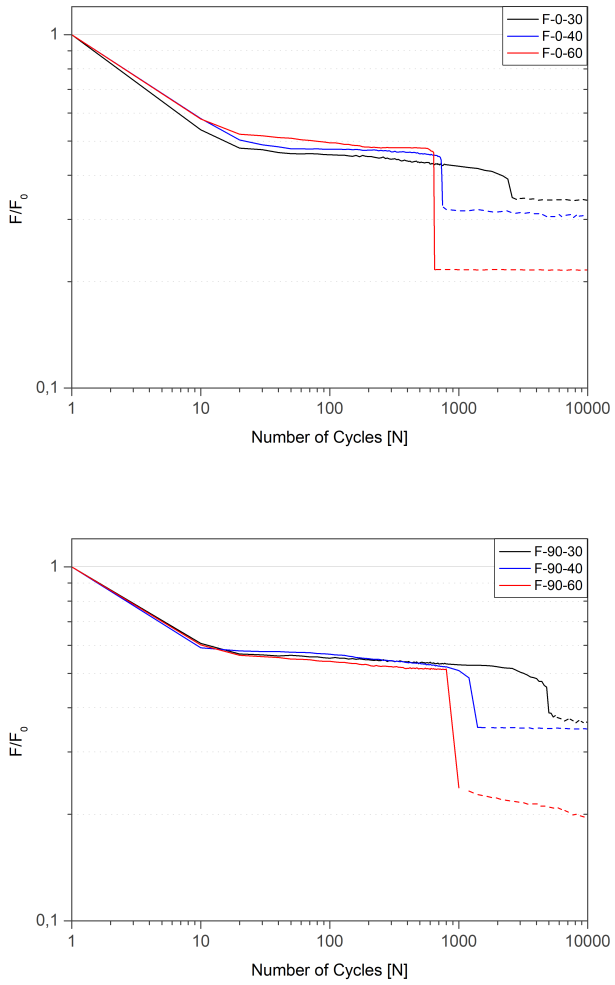

Figure 7.24: Fatigue effect on Load versus number of cycles.

Comparing the curves of the load versus number of cycles for each of the specimen type, in Table 7.9 is presented the fatigue effect in each of the respective normalized loads, up the the moment of ultimate failure.

Table 7.9: Comparison of the fatigue effects in the load of each specimen type.

Specimens	Load decrease (%)
F-0-30	66.2
F-0-40	69.9
F-0-60	79.5
F-90-30	60.2
F-90-40	66.5
F-90-60	83.1

According to the table, it is possible to state that the effect of fatigue is proportional to the increase of the patch size, for both laminates' stacking sequence. This is in agreement with the failure mechanism that the specimens suffer. The stiffness difference between the specimen types is fully dependent on their patch size, as the parent plate is common to all the specimens. Therefore, once the structure experiences delamination, either in

the patch or in the outermost ply of the parent plate, this leads to a significant drop on the stiffness, reaching a value somehow similar to the stiffness of the originally notched laminate. Knowing that the bigger the patch, the higher the bending stiffness, this will influence the percentage of stiffness that is lost by the effect of fatigue, that in turn, will be proportional to the percentage drop of the load.

Finally, the comparison of fatigue life for each patch size in shown in Figure 7.25, where the average tendency line is presented for each stacking sequence relatively to the number of cycles up to ultimate failure that each specimen was able to endure before ultimate failure. It is clear that with the increase of the patch size the fatigue life of both the 0º and 90º specimens decreases.this is due to the increase of the stiffness that leads the structure to a rearrangement of the peel stresses concentrations and the structure becomes propitious to the propagation of cracks, which explains the smaller fatigue life.

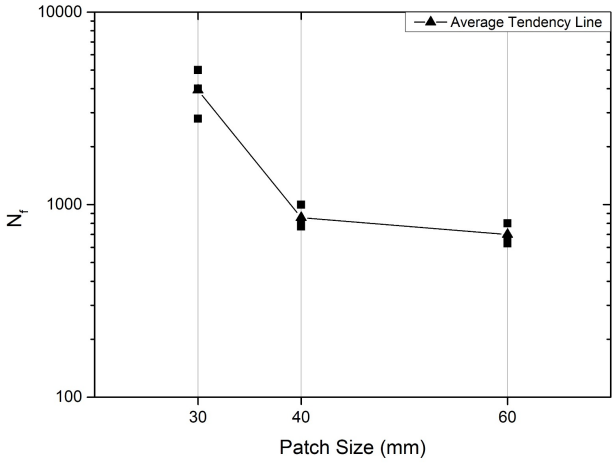

(a)

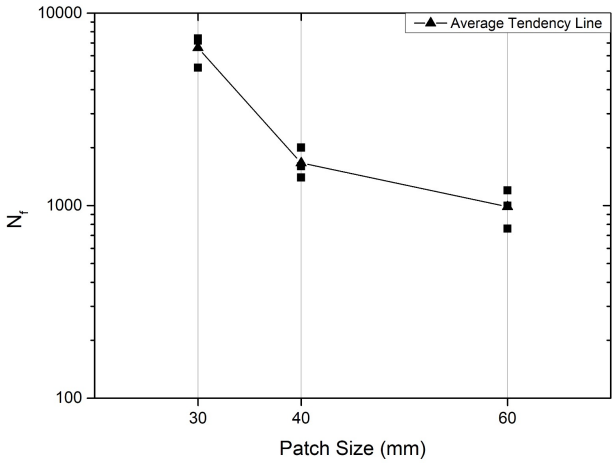

(b)

Figure 7.25: Average number of fatigue cycles for each patch size: (a) 0º specimens; (b) 90º specimens.

Chapter 8

Final Conclusions and Future Works

The flexural analysis of the mechanical performance of single patch repairs was studied and discussed in the previous chapter and the final conclusions will be addressed in this section. Possible future works will also be suggested in order to improve the study and develop it in specific aspects that allow the optimization of the structure.

Conclusions

This work was made in order to optimize two main variables of the structures' geometry and the effects of this changes on the performance of the structure when experimentally tested in quasi-static and fatigue modes. The specimens were also subjected to low-velocity impact in order to study their residual properties.

The effect of the stacking sequence of the CFRP parent, notched, repaired and impacted laminates and the effect of the patch dimension (30, 40 and 60 mm) for each stacking sequence on the stiffness and load-carrying performance were analyzed in detail.

From this study it was possible to conclude that the 100 mm x 150 mm parent laminate is sensible to a open hole of 20 mm diameter. The effect of the hole on the stiffness of the laminate was proven to be similar, for both the stacking sequences.

For the 0º specimens, with a stacking sequence of $[0,90,0,90,0,90]_S$ and an open hole of 20 mm diameter, and according to the quasi-static tests, the 60 mm patch was the only one shown to be effective in restoring the mechanical properties of the parent laminate. This overlap length was also proven to be beneficial when studying the residual properties of the impacted laminate, as it was the one with less relative damaged area and consequent better performance. This repair geometry was able to keep a load-carrying capacity higher than the one from the parent laminate, even after damage. This can be considered a possible on-site repair even if the parent plate has no damage, because the laminate performance will be improved.

For the 90º specimens, $[90,0,90,0,90,0]_S$, none of the repairs was able to achieve the mechanical properties of the parent laminate, however the improvement of the properties was shown to be proportional to the increase of the patch size.

The improvement of both the stiffness and consequent increase of capacity of the specimens to support higher loads is important, even if it doesn't represent an effective repair, because this shows that the increase of the stiffness for the studied patch sizes proportionally affects the load-carrying capacity.

On the other hand, for the dynamic tests, the results were contrary, as the fatigue life of both specimen types was inversely proportional to the increase of patch size. The 30 mm patch repair specimens endured more fatigue cycles than the others, which is justified by the lowest stiffness of the structure. When increasing the stiffness, the peeling stresses concentrated in the edges of the patch intensify, becoming favorable to the propagation of cracks and exposed to the effects of fatigue.

Future Works

The work performed in this thesis can be improved and continued in several aspects. For instance, other patch sizes could be studied in order to find the optimal geometry for each of the stacking sequences. Even though the 60 mm patch was found to be an effective repair for the 0º laminates, there is still room for optimization in order to achieve an ideal temporary repair geometry that assures the functionality and strength of the structure. Following the same optimization goal, a functional patch repair is still to be found for the 90º laminates. Larger patches, than the ones already studied, must be tested in order to find the minimum ratio of patch size and damage/hole size, for each structure.

It should also be noted that the notch sensitivity studies were limited to a single hole diameter, which may influence the performance of the patches in case of a different D/W value. This is a variable that can also be studied in more depth. The 0/90 layup is not commonly used in real life applications, however it was chosen in this study as it represents the worst case scenario when affected by damage or notches. This sensitivity can be overcome in real life applications by resorting to quasi-static layups and study them and their repair methods, which can be done using numerical models.

The results obtained from the quasi-static and fatigue studies were opposed, which

reveals the need of a deeper numerical study in order to achieve an equipoise between both performances. In this study the numerical analysis was validated, however it can be extended as well to be validated by introducing failure criteria and damage propagation laws. Once this results are compared and confirmed with the experimental work, the method will be reliable enough to do a parametric study on the effect of the patch size to the damage size. This will allow to reach an optimal patch size-hole diameter ratio.

Appendix A

Adhesive Datasheet

3M™ Scotch-Weld™ 9323 B/A

Two Part Structural Adhesive

Product Description

3M™ Scotch-Weld™ Structural Epoxy Adhesive 9323 B/A is a two component epoxy adhesive which cures at room temperature or with mild heat to form a tough, impact resistant structural bond. It has an excellent adhesion to a wide variety of substrates such as metals, glass, ceramics and plastics, incl. GFRP and CFRP. Once cured it provides extremely high shear and peel strength over a wide temperature range, with outstanding resistance to harsh environments and chemicals commonly encountered in aerospace applications.

Key Features

- Toughened system providing extremely high shear and peel strength
- Wide service temperature range
- Outstanding environmental resistance
- Full room temperature processing

Product Characterization

The following technical information and data should be considered representative or typical only and should not be used for specification purpose

General Properties	Part B	Part A
Colour	Off-white	Red-orange
Base	Modified epoxy	Modified amine
Consistency	Thixotropic paste	Slight gel
Density	1.18 g / cm³	1.06 g / cm³
Solids	100 %	100 %
Viscosity [A]	1000 – 2000 Pas	10 – 25 Pas
Mix ratio by weight (by volume)	100 : 27 (100 : 30)	
Work life [B] at 23 ± 2 °C / Open Time	150 minutes / 20 minutes	
Strength build-up at 23 ± 2 °C	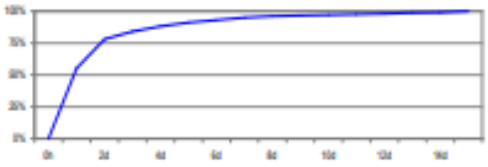	
Handling strength [C]	4-5 hours	
Full cure cycle	14 days at room temperature	
Packaging	Cans and pails	

[A] Brookfield RVF Spindle 7,2 Upm [B] 50 g of mixed adhesive [C] Time to reach 1 MPa Shear Strength

Product Performance

The following data show typical values obtained with Scotch-Weld™ 9323 B/A on unprimed, sulfochromic etched, 2024 T3 aluminium. The samples have been cured for 15 days at room temperature, if not stated otherwise. To control the bond line thickness, approximately 1 wt. % of glass beads, 90 – 150 µm diameter were added to the adhesive.

Mechanical Properties		Test Temperature	Cured for 15 days at 23 °C	Cured for 2 hours at 65 °C
Overlap Shear Strength EN 2243-1		-55 °C	38 MPa	42 MPa
		23 °C	36 MPa	40 MPa
		80 °C	22 MPa	22 MPa
		120 °C	4 MPa	4 MPa
		150 °C	2 MPa	-
Overlap Shear Strength EN 2243-1	Stainless steel	23 °C	-	27 MPa
	CFRP, GFRP epoxy matrix resin	23 °C	-	28 MPa [a]
	PMMA	23 °C	-	3 MPa [a]
Floating Roller Peel Strength EN 2243-2		-55 °C	120 N / 25 mm	90 N / 25 mm
		23 °C	170 N / 25 mm	190 N / 25 mm
		80 °C	145 N / 25 mm	145 N / 25 mm
Impact Resistance AFNOR NF 76-115		23 °C	17,4 kJ / m²	32,2 kJ / m²

[a] Substrate Failure

Environmental Ageing

The following data show typical values obtained with Scotch-Weld 9323 B/A after 750 hours exposure to different media and environments to determine the aging resistance. The samples have been cured for 15 days at room temperature.

Mechanical Properties	Environment	Test Temperature	Results
Overlap Shear Strength EN 2243-1	Demineralized water at 23 ± 2 °C	23 °C	34 MPa
	Gasoline super at 23 ± 2 °C	23 °C	36 MPa
	Engine oil (20W40) 23 ± 2 °C	23 °C	36 MPa
	Hydraulic fluid skydrol 500B at 23 ± 2 °C	23 °C	37 MPa
	JP4 fluid at 23 ± 2 °C	23 °C	36 MPa
	5 % Salt spray at 23 ± 2 °C	23 °C	34 MPa
	Hot / Wet 70 °C, ≥ 95% R.H.	23 °C	33 MPa
	Dry heat at 120 ± 2 °C	23 °C	35 MPa

3M™ Scotch-Weld™ Structural Epoxy Adhesive 9323-150 B/A

Scotch-Weld™ 9323-150 B/A is a product modification of Scotch-Weld™ 9323 B/A. There are no significant differences in terms of performance. It contains 1 wt % of glass beads 90 – 150 µm diameter for bond line thickness control. Slight differences can be observed in density and viscosity.

Handling, Application, Storage

Precautionary Information

Refer to product label and Material Safety Data Sheet (MSDS) for health and safety information before using this product. For MSDS visit our website www.3M.com/msds.

Instructions for use

While this information is provided as general application guideline based upon typical conditions, it is recognized that no two applications are identical due to, among other things, differing assemblies, methods of heat and pressure application, production equipment and other limitations. It is therefore suggested that experiments be run, within the actual constrains imposed to determine optimum conditions for your specific application and to determine suitability of product for particular intended use.

Process step	Instruction
Surface preparation	The strength and durability of a bonded joint are dependent on proper treatment of the surface to be bonded. An acclimated, thoroughly cleaned, dry, grease-free surface is essential for maximum performance. Cleaning methods which will produce a break free water film on metal surfaces are generally satisfactory. At the very least, joint surfaces should be cleaned with a good proprietary degreasing agent and mechanically abraded, e.g. with 3M Scotch-Brite™ 7447. Abrading should be followed by a second degreasing treatment, e.g. with 3M 08984 Adhesive Cleaner. Optimum processing temperature for substrates and adhesive is around room temperature of 23 °C.
Application	This product consists of two parts. Combine Part B and Part A in a separate container just prior to application in the proportions specified. **Note:** Mix ratio deviations above +/- 5 % have significant influence on material performance. Mix both components thoroughly until a uniform colour is obtained. **Important:** Be careful when mixing quantities larger than 100 grams, because exothermic reaction may occur. Apply adhesive to parts to be bonded before the work life expires, e.g. by spatula. **Note:** Work life depends to some extent on mixed quantity and the shape of the container. Use of a shallow container will minimize the quantity impact. In order to obtain optimum mechanical performance, the joint components should be assembled and clamped as soon as the adhesive has been applied and before end of the open time. A fixation of the joint and an even contact pressure throughout the joint area during cure will ensure optimum performance. Maximum shear strength is obtained with 0.10 – 0.20 mm bond line thickness. Close the containers after use to protect the material against humidity.
Curing	Once mixed, Scotch-Weld™ 9323 B/A will gel in 3 hours, build up handling strength in 4-5 hours and fully cure within 14 days at room temperature. **Note:** Lower temperature will slow down the reaction times. Curing time can be accelerated by mild heat. Following times and temperatures will result in a full cure: • 14 days at 23 ± 2 °C • 2 hours at 65 ± 2 °C • 15 minutes at 100 ± 2 °C **Note:** The curing temperature may have influence on the final product performance.
Cleaning	Excess uncured adhesive can be cleaned with ketone type solvents. After cure the adhesive can be removed mechanically. **Note:** When using solvents, extinguish all ignition sources, including pilot lights, and follow the manufacturer's precautions and instructions for use.
Storage and Handling	Store the product at room temperature. Shelf life is 12 months from date of shipment in the original unopened containers.

Aerospace and Aircraft Maintenance Department
European Aerospace Laboratory
www.3m.eu/aerospace

Reference: 104

Appendix B

Repaired Specimen Views

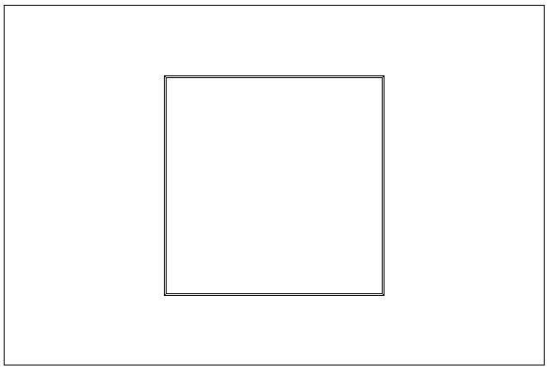

Top View

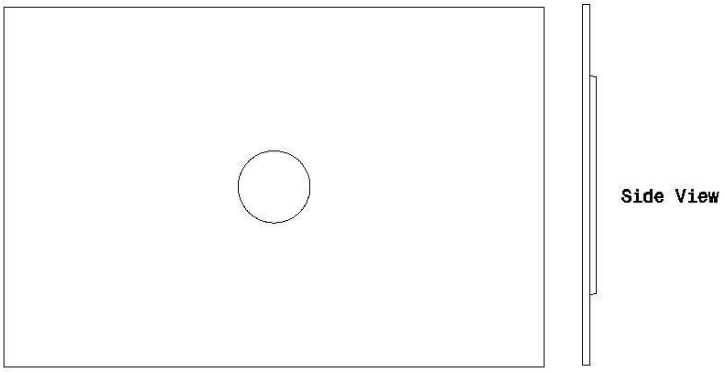

Bottom View

Appendix C

Equations for D Matrix Calculation

In order to calculate the bending stiffness, the reduced stiffness matrix of the material, Q, is calculated and corresponds to the elastic behavior of the ply in the plane loading :

$$Q = \frac{E_{11}^2}{(E_{11} - \upsilon_{12}) * E_{22}} \quad \text{(C.1)}$$

This equation corresponds to this specific study as only one material was used. From this matrix, it is possible to calculate the extensional stiffness matrix,A_{ij}, coupling stiffness matrix,B_{ij}, and finally the bending stiffness,D_{ij},:

$$A_{ij} = \sum_{k=1}^{n} \{Q_{ij}\}_n (z_n - z_{k-1}) \quad \text{(C.2)}$$

$$B_{ij} = \frac{1}{2} \sum_{k=1}^{n} \{Q_{ij}\}_n (z_n^2 - z_{k-1}^2) \quad \text{(C.3)}$$

$$D_{ij} = \frac{1}{3} \sum_{k=1}^{n} \{Q_{ij}\}_n (z_n^3 - z_{k-1}^3) \quad \text{(C.4)}$$